HHS Public Access

Author manuscript

Cell Rep. Author manuscript; available in PMC 2024 March 28.

Published in final edited form as:

Cell Rep. 2024 February 27; 43(2): 113680. doi:10.1016/j.celrep.2024.113680.

Notch receptor-ligand binding facilitates extracellular vesicle-mediated neuron-to-neuron communication

Yi-Zhi Wang[1], **Charlotte C.M. Castillon**[2], **Kamil K. Gebis**[1], **Elizabeth T. Bartom**[3], **Alessandra d'Azzo**[4], **Anis Contractor**[2], **Jeffrey N. Savas**[1,5,*]

[1]Department of Neurology, Northwestern University Feinberg School of Medicine, Chicago, IL 60611, USA

[2]Department of Neuroscience, Northwestern University Feinberg School of Medicine, Chicago, IL 60611, USA

[3]Department of Biochemistry and Molecular Genetics, Northwestern University Feinberg School of Medicine, Chicago, IL 60611, USA

[4]Department of Genetics, St Jude Children's Research Hospital, Memphis, TN 38105, USA

[5]Lead contact

SUMMARY

Extracellular vesicles (EVs) facilitate intercellular communication by transferring cargo between cells in a variety of tissues. However, how EVs achieve cell-type-specific intercellular communication is still largely unknown. We found that Notch1 and Notch2 proteins are expressed on the surface of neuronal EVs that have been generated in response to neuronal excitatory synaptic activity. Notch ligands bind these EVs on the neuronal plasma membrane, trigger their internalization, activate the Notch signaling pathway, and drive the expression of Notch target genes. The generation of these neuronal EVs requires the endosomal sorting complex required for transport-associated protein Alix. Adult Alix conditional knockout mice have reduced hippocampal Notch signaling activation and glutamatergic synaptic protein expression. Thus, EVs facilitate neuron-to-neuron communication via the Notch receptor-ligand system in the brain.

In brief

Wang et al. show that excitatory synaptic activity triggers the release of extracellular vesicles (EVs). They found Notch1 and Notch2 proteins on the surface of EVs. The Notch ligand-receptor

*Correspondence: jeffrey.savas@northwestern.edu.

AUTHOR CONTRIBUTIONS

Y.-Z.W., A.C., and J.N.S. designed the experiments. Y.-Z.W. and J.N.S. wrote the manuscript. Y.-Z.W. performed EV purification and IHC and ICC experiments. Y.-Z.W. and K.K.G. performed all biochemical and MS experiments. C.C.M.C. performed all electrophysiological experiments and related data analysis. E.T.B. performed RNA sequencing data analysis. Y.-Z.W. performed the analyses of biochemical, IHC, ICC, and MS experiments. A.d'A. provided the *Alix*$^{-/-}$ mice.

DECLARATION OF INTERESTS

The authors declare no competing financial interests.

SUPPLEMENTAL INFORMATION

Supplemental information can be found online at https://doi.org/10.1016/j.celrep.2024.113680.

system plays a key role in promoting the selective uptake of these EVs by neurons, thereby mediating unconventional neuron-to-neuron communication.

Graphical Abstract

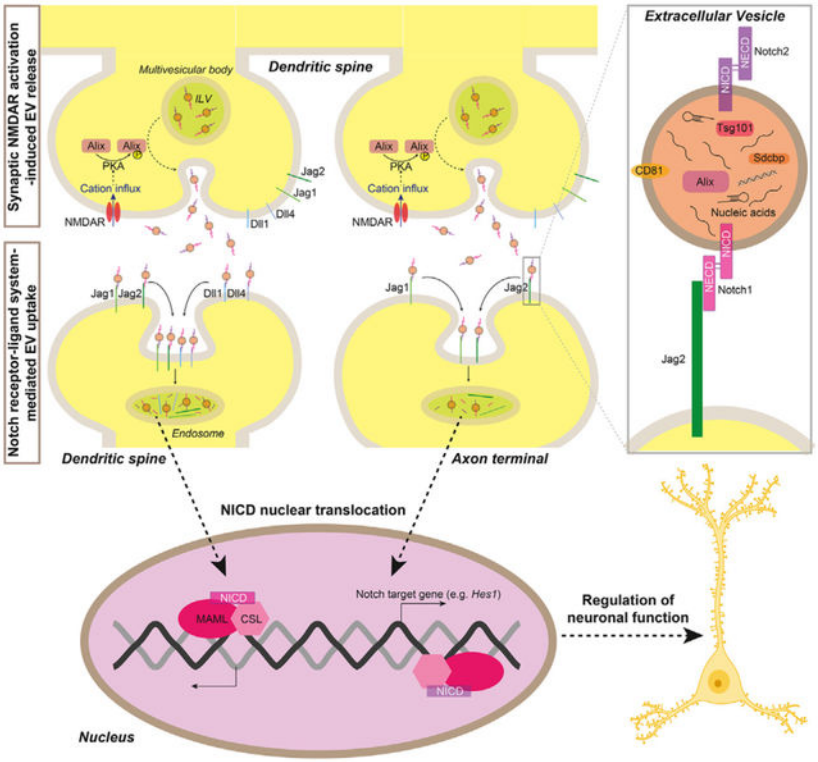

INTRODUCTION

Neurons communicate with each other by selectively sending and receiving chemical and electrical signals. Recently, extracellular vesicles (EVs) have emerged as additional potential mediators of intercellular communication in the central nervous system (CNS).[1,2] EVs are nanosized particles composed of lipids, proteins, and nucleic acids.[3–5] Originally, EVs were thought to function primarily in the mass removal of unwanted cellular by-products and waste, removing them from cells by secretion into the extracellular space.[6] However, a substantial body of recent results challenges these findings and supports a key role for EV-based intercellular signaling. For instance, neurons release EVs in response to various forms of synaptic plasticity and during brain development.[7–11] Furthermore, additional evidence indicates that CNS EVs facilitate cell-type-specific cargo transfer.[4] Specifically, activation of glutamate receptors triggers neurons and oligodendrocytes to release EVs, and these EVs are selectively internalized by neurons.[12–14] On the other hand, unstimulated oligodendrocytes release EVs that are preferentially transferred to microglia.[15] Despite these observations, skepticism about the biological significance of EV-mediated cell-to-cell communication in the CNS has persisted. This study aims to expand the knowledge of the

molecular mechanisms underlying cell-type-specific EV-based intercellular communication and to identify an EV receptor system in the CNS.

RESULTS

NMDAR activity-induced EVs contain Notch1 and Notch2 proteins

We set out to identify proteins responsible for mediating cell-type-specific EV communication using cultured rodent neurons. Neuronal EV biogenesis and release was triggered by activating synaptic N-methyl-D-aspartate receptors (NMDARs) with a Mg^{2+}-free glycine solution[16] (Figures 1A and S1A–S1I). We isolated neuronal EVs using a previously developed isolation strategy based on size exclusion chromatography (SEC)[17] (Figure 1A). Negative staining electron microscopy (EM) analysis revealed abundant EV-like particles in the second SEC fraction isolated from the Mg^{2+}-free glycine solution used to stimulate the neurons (Figures 1B, 1C, S1J, and S1K). Western blot (WB) analysis confirmed that this fraction was enriched for three EV markers—Alix, Tsg101, and CD81—but not for GM130, a protein located in the Golgi apparatus (Figure 1D).

All ten SEC fractions were individually analyzed with liquid chromatography-tandem mass spectrometry (LC-MS/MS)-based proteomics (Figure 1E). We identified 114 proteins with significantly higher levels in EV-enriched fraction, relative to the other fractions (Table S1). Gene Ontology enrichment analysis revealed robust enrichment of proteins associated with EVs (Table S1), including 60 canonical EV markers (e.g., endosomal sorting complex required for transport [ESCRT] complex proteins and tetraspanins).[3,5] Among the additional 54 proteins, Notch1 and Notch2 stood out as prominent candidates for specifying EV binding, because they are transmembrane proteins that are captured by high-affinity ligands.[18,19] Notably, the identified Notch1 and Notch2 peptides mapped to both the extra- and intracellular domains (ECDs or ICDs, respectively). Thus Notch1 and Notch2 in these EVs have not been activated by proteolytic cleavage (Figure 1E).[18] WB analysis of SEC fractions confirmed the presence of $Notch1_{ICD}$ and $Notch2_{ICD}$ in EVs but failed to detect activated Notch1, activated Notch2, or the Notch ligands Jag1, Jag2, Dll1, and Dll4 (Figure 1F).

Neurons internalize EVs using Notch ligands

The canonical Notch signaling pathway begins at the cell surface by the binding of $Notch_{ECD}$ to transmembrane ligands.[18,19] Likewise, if $Notch_{ECD}$ is present on the EV surface, it could also bind Notch ligands expressed on the neuronal plasma membrane to activate signaling. To investigate how Notch is orientated within the EV membrane, we incubated purified EVs with proteinase K (PK) to digest peptide bonds accessible on the EV surface. We then used $Notch1_{ICD}$ and $Notch2_{ICD}$ antibodies and WB analysis to determine which Notch protein domains are protected from digestion within the EV lumen. Notably, PK treatment reduced both Notch1 and Notch2 molecular weight by ~10 kDa, consistent with the removal of the extracellular domain of $Notch_{ICD}$, which anchors the $Notch_{ECD}$ (Figure 2A). Thus, $Notch_{ECD}$ is present on the EV surface (Figure 2B). By contrast, PK readily digested the multi-pass transmembrane EV protein CD81 but did not digest the EV luminal protein Sdcbp.[20]

The binding of $Notch_{ECD}$ to Notch ligands leads to the internalization of the ligand-receptor complex into the acceptor cell.[18,19] Thus, we hypothesized that EVs containing $Notch_{ECD}$ on their surface may also be internalized. If so, internalized EVs should remain punctate after internalization, and Notch ligands should colocalize with the internalized EVs. To test this hypothesis, we labeled neuronal EVs with the protein dye carboxyfluorescein succinimidyl ester (CFSE) to track internalized EVs. Visualization of the CFSE signals in neurons revealed that internalized EV proteins remain concentrated in puncta, which colocalize with Notch ligands, especially Jag1, in neuronal soma and dendrites (Figures 2C and 2D). We also found that Jag1, Jag2, Dll1, and Dll4 are predominantly expressed by cultured rat hippocampal neurons[21] (Figure S2A). Immunocytochemistry (ICC) analysis indicates that Notch ligands partially colocalize with VGlut1 and Homer1, glutamatergic presynaptic and postsynaptic markers, respectively (Figures S2B and S2C). Furthermore, Notch1 and Notch2 proteins also partially colocalize with VGlut1 and the excitatory postsynaptic marker PSD95 (Figure S2D). However, our ability to discern pre- or postsynaptic colocalization is limited, and even VGlut1 and Homer1 signals exhibit some colocalization (Figure S2B). To further investigate the synaptic localization of Notch1 and Notch2 proteins, we examined subcellular biochemical fractions of mouse cortex by WB analysis (Figure S2E). We found that $Notch1_{ICD}$, $Notch2_{ICD}$, Dll1, and Dll4 are enriched within the postsynaptic density (PSD) and are nearly absent in the presynaptic (Pre) fractions. Notably, Jag1 and Jag2 are detected in both the Pre and PSD fractions. Thus, glutamatergic axon terminals and dendritic spines, which are hotspots of endocytosis,[22–24] may represent active sites for EV internalization. We also detected the canonical EV proteins, tsg101, Alix, and Sdcbp, in the PSD fraction but not in the Pre fraction. This finding strongly suggests that dendritic spines are the primary sites for EV release. We also used live-cell imaging to confirm that EVs were predominantly released from dendritic spines (Figures S2F–S2H), consistent with previous findings.[7,14]

To investigate whether EVs directly fuse with the neuronal plasma membrane, which does not require endocytosis, we labeled EVs with the lipophilic dye CM-Dil. The CM-Dil-labeled EVs were observed in a punctate pattern after internalization (Figure S3A). This suggests that EV membrane integrity is maintained after internalization, rather than directly fusing with neuronal plasma membrane. Furthermore, CFSE-labeled EVs are selectively internalized by MAP2-positive neurons (Figures S3B and S3C). To corroborate this finding, we acquired a Notch1 expression construct containing a C-terminal myc epitope tag.[25] We packaged this construct into lentiviruses, infected neurons, and then harvested glycine-induced EVs. Next, we treated additional non-infected neurons with EVs containing C-terminal myc-tagged Notch1 (Figure S3D). Consistently, the majority of myc signal was observed within MAP2-positive neurons, and some myc signal was punctate, while other myc signal was highly enriched in the nucleus (Figure S3E). This observation provides evidence that $Notch_{ICD}$ from EVs can translocate into the nucleus of recipient neurons. Notably, EVs incubated with PK were not detected in neurons, which further supports a role for NECD-ligand *trans* interaction in mediating target specificity (Figures 2E and S3F).

In light of the aforementioned observations, we hypothesized that the internalization of EVs alone has the potential to activate the expression of Notch target genes, such as *Hes1*.[18,19] To test whether $Notch_{ICD}$ within EVs is functional, we spiked neuronal cultures with these EVs

and examined the activation of the Notch pathway by WB. In support of this hypothesis, the levels of activated Notch1, activated Notch2, and Hes1 proteins were all significantly elevated in neurons incubated with the EVs (Figures 2F–2I and S3G–S3J). In contrast, EVs pretreated with PK failed to activate the Notch signaling pathway. To confirm that EV Notch proteins are responsible for activation of Notch signaling in recipient neurons, we next incubated the Notch EVs with the synthetic peptide Delta^{MAX}. Delta^{MAX} has very high binding affinity for murine Notch ECD and can be used to interfere with ligand-receptor binding.[26] We found that EVs preincubated with Delta^{MAX} were unable to initiate the Notch signaling pathway (Figures 2F–2I). To investigate if Notch EVs impact neuronal morphology, we incubated cultured neurons with the EVs for 1 h and found that they significantly increased spine density (Figures S4A and S4B), suggesting EVs play a role in regulating the morphology of dendritic spines.[27] Taken together, Notch$_{ICD}$ within EVs can be further processed and can drive *Hes1* gene expression.

Activation of synaptic NMDARs leads to Notch target gene expression

To examine whether endogenous neuronal EV-mediated communication is sufficient to trigger Notch signaling in nearby neurons, we again stimulated cultured rat hippocampal neurons with vehicle (Veh) or Mg^{2+}-free glycine. In this experiment, instead of purifying EVs, we harvested the neuronal RNA at multiple time points after treatment and performed bulk poly-A RNA sequencing to examine changes in gene expression (Figure 3A; Table S2). Interestingly, we found that synaptic NMDAR activation significantly induced expression of multiple Notch target genes (e.g., *Hes1* and *Nrarp*) 60 min after treatment (Figures 3B and 3C; Table S2). Additionally, this stimulation also increased the level of activated Notch1, Notch 2, and Hes1 proteins (Figures 3D and 3E). This effect was inhibited by the NMDAR antagonist D-2-amino-5-phosphonovalerate (APV). Thus, at least in this system, activation of the Notch signaling pathway is NMDAR dependent.[28] Furthermore, inhibiting endocytosis with dynasore blocked elevation of activated Notch1, activated Notch2, and Hes1 protein levels, suggesting internalization of EVs is required for Notch signaling pathway activation (Figures 3D and 3E).[29,30] Altogether, these data strongly suggest endogenously released neuronal EVs are sufficient to activate the Notch signaling pathway.

Synaptic NMDAR activation of the EV Notch signaling pathway requires Alix expression

We next hypothesized that neurons with impaired EV biogenesis/release machinery are unable to activate the NMDAR-based EV signaling pathway. Alix (encoded by *Pdcd6ip* gene) functions in the ESCRT pathway and is essential for EV biogenesis and release in multiple cell lines,[31,32] so we suspected that Alix may also play a critical role in neuronal EV release. Consistently, activation of synaptic NMDARs induced significantly fewer EVs to be released from *Alix* $^{+/-}$ and *Alix*$^{-/-}$ neurons[33] (Figures 4A andS4C–S4E). We also failed to detect any Notch proteins or known EV protein markers in the SEC fractions by WB (Figure 4B). These results show that Alix is required for synaptic NMDAR activation-induced EV release. Moreover, as hypothesized, Mg^{2+}-free glycine stimulation failed to increase activated-Notch1, activated-Notch2, or Hes1 protein levels in *Alix*$^{-/-}$ neurons (Figures 4C–4F). Besides regulating EV release, Alix also contributes to protein cargo transport from early endosomes to multivesicular bodies (MVBs).[34–37] Therefore, we next examined whether the lack of Notch signaling pathway activation in *Alix*$^{-/-}$ neurons

is due to disruption of intracellular Notch protein trafficking. We found that Alix deletion only slightly reduced Notch1 levels at Tsg101-[38] and lysobisphosphatidic acid-positive puncta (i.e., MVBs and late endosomes respectively) (Figures S4F and S4G). These mild changes suggest Notch protein trafficking is only marginally altered in *Alix*$^{-/-}$ neurons. This alteration may be a mechanism underlying the abnormal embryonic brain development in *Alix*$^{-/-}$ mice, which results from neuronal precursor apoptosis.[33,39,40]

Synaptic NMDAR activation triggers Alix phosphorylation to facilitate EV release

We next investigated how activation of synaptic NMDARs promotes EV release and engages the Notch signaling pathway. Under basal conditions, Alix activity is suppressed by conformational autoinhibition through the interaction of proline-rich region (PRR) and BRO-domain-containing protein (BRO) domains.[41,42] In tumor cells, phosphorylation of Alix disrupts the PRR-BRO interaction and facilitates cytokinetic abscission and retroviral budding.[41] This led us to suspect that Alix phosphorylation may also be required for EV release induced by synaptic activity. NMDAR activation led to Alix phosphorylation and was blocked by APV (Figures S5A–S5C). Protein kinase A (PKA), protein kinase C (PKC), and Ca^{2+}/calmodulin-dependent protein kinase II (Camk2) are engaged after activation of synaptic NMDARs.[43] Thus, we tested four kinase inhibitors and found only the PKA inhibitor H89 can significantly inhibit Alix phosphorylation (Figures 4G, 4H, and S5D). Additionally, both APV and H89 can suppress NMDAR activity-induced EV release (Figure S5E), which suggests both NMDAR and PKA are required for Mg^{2+}-free glycine stimulation-induced EV release. To identify candidate Alix phosphorylation site(s) required for EV release, we performed LC-MS/MS analysis of neurons treated with Mg^{2+}-free glycine or vehicle solutions and found that Alix is phosphorylated at serine 717 (S717) (Figure 4I). No phosphorylated Alix peptides were identified in vehicle-treated neurons. S717 localizes to the junction between the V-domain and the PRR domain (Figure 4J), which is evolutionarily conserved among animals (Table S3). To test whether phosphorylation of S717 contributes to NMDAR activity-induced EV release, we mutated the serine to aspartic acid (S717D) to mimic constitutive phosphorylation. We also constructed a phosphorylation-dead mutant by replacing the serine with alanine (S717A). We then packaged these two constructs into lentiviruses and infected *Alix*$^{-/-}$ hippocampal neurons. Overexpression of mCherry-Alix or mCherry-Alix-S717D, but not mCherry or mCherry-Alix-S717A, successfully rescued NMDAR activity-induced EV release (Figures 4K, 4L, S5F, and S5G). Altogether, these data provide strong evidence that Alix phosphorylation plays a critical role in synaptic NMDAR activation-induced EV release.

Notch signaling is reduced in adult *Alix*$^{-/-}$ mouse hippocampus

Alix is a multifunctional protein that is associated with the ESCRT machinery and plays a key role in several membrane-centric processes. For example are membrane repair, MVB and exosome biogenesis, and neuronal activity-dependent bulk endocytosis.[44] Since bulk endocytosis is an important mechanism that facilitates EV uptake,[4] *Alix*$^{-/-}$ neurons may also have hampered EV internalization. Therefore, *Alix*$^{-/-}$ mice have severely hampered EV processes, and we hypothesized that the EV Notch signaling pathway is also impaired. During the very early stages of postnatal brain development (i.e., post-natal day [P]0–P4),

there is nearly no excitatory synaptic transmission in the brain.[45,46] Consistently the level of $Notch1_{ICD}$, $Notch2_{ICD}$, activated Notch1, activated Notch2, and Hes1 proteins are very similar in *Alix*$^{+/+}$ and *Alix*$^{-/-}$ hippocampal extracts (Figures 5A and 5B). In contrast, at P14, when excitatory synaptic transmission is established, the levels of activated Notch1, activated Notch2, and Hes1 proteins in *Alix*$^{+/+}$ hippocampus are significantly higher than in *Alix*$^{-/-}$ hippocampus (Figures 5A and 5B). However, the levels of $Notch1_{ICD}$ and $Notch2_{ICD}$ remain similar.

$Notch_{ICD}$ translocates to the nucleus to induce expression of Notch target genes.[18,19] Thus, the degree of Notch signaling pathway activation is correlated with the abundance of nuclear $Notch_{ICD}$. At P0 and P4, the expression patterns of $Notch1_{ICD}$ and $Notch2_{ICD}$ are very similar in *Alix*$^{+/+}$ and *Alix*$^{-/-}$ hippocampi (Figures 5C and S6). However, at P14, there is less nuclear $Notch1_{ICD}$ and $Notch2_{ICD}$ in *Alix*$^{-/-}$ hippocampal CA1 and CA3 regions compared to *Alix*$^{+/+}$ hippocampus. There was also less $Notch1_{ICD}$ in P14 *Alix*$^{-/-}$ dentate gyrus (DG). Notably, the expression patterns of $Notch2_{ICD}$ are very similar in *Alix*$^{+/+}$ and *Alix*$^{-/-}$ DGs (Figures 5C and S6B). Therefore, our data strongly suggest that Notch pathway activation is associated with the developmental onset of excitatory synaptic transmission and that impaired neuronal EV-based signaling decreases Notch pathway activation in the mouse hippocampus.

Alix is required for activation of the Notch signaling pathway in the adult mouse hippocampus

Alix plays important roles in brain development, and *Alix*$^{-/-}$ mouse brains are significantly smaller compared to wild type.[33,39,44] To avoid the defects in embryonic development, we crossed *Alix-floxed* (*Alix*$^{fl/fl}$) mice with *Camk2a-cre* mice to obtain *Camk2a-cre::Alix*$^{fl/fl}$. *Camk2a-cre* is highly expressed in pyramidal neurons of adult mouse hippocampus and turns on around P30. At P60, Alix protein levels in *Camk2a-cre::Alix*$^{fl/fl}$ hippocampus were reduced to ~5% of the level in *Alix*$^{fl/fl}$ hippocampus (Figures 6A and 6B). The level of activated Notch1, activated Notch2, and Hes1 proteins were also significantly reduced in *Camk2a-cre::Alix*$^{fl/fl}$ hippocampus compared to *Alix*$^{fl/fl}$ hippocampus. However, $Notch1_{ICD}$ and $Notch2_{ICD}$ protein levels remained similar, suggesting the reduction is not due to downregulation of Notch protein expression.

We further examined the expression patterns of $Notch1_{ICD}$ and $Notch2_{ICD}$ in *Alix*$^{fl/fl}$ and *Camk2a-cre::Alix*$^{fl/fl}$ hippocampi (Figures 6C and 6D). Compared to *Alix*$^{fl/fl}$ hippocampus, the amount of nuclear $Notch1_{ICD}$ was significantly reduced in Alix conditional knockout (cKO) CA1, CA3, and DG regions. By contrast, cKO of Alix significantly reduced the amount of nuclear $Notch2_{ICD}$ in CA1 and CA3 but not DG. This region-specific alteration of $Notch1_{ICD}$ and $Notch2_{ICD}$ expression patterns suggests Notch1 and Notch2 may exist in separate populations of neuronal EVs and are released by different neurons. Collectively, these data strongly suggest that hampered neuronal EV release limits activation of the Notch pathway in the adult brain.

Conditional deletion of Alix in the adult mouse brain leads to hippocampal subregion-specific proteomic changes

The Notch signaling pathway plays important roles in synaptic function.[21,28,47–49] To investigate the consequences of reduced Notch signaling activity in the mouse hippocampus, we used tandem mass tag (TMT)-based proteomic analysis to quantitatively compare the *Alix*$^{fl/fl}$ and *Camk2a-cre::Alix*$^{fl/fl}$ hippocampal CA1, CA3, and DG proteomes respectively (Figures 7 and S7; Table S4). The conditional deletion of Alix leads to distinct proteomic changes in CA1, CA3, and DG (Figures 7B and 7C). This finding aligns with the region-specific changes in Notch1$_{ICD}$ and Notch2$_{ICD}$ levels within the hippocampus of *Camk2a-cre::Alix*$^{fl/fl}$ brain (Figures 6C and 6D). Notably, the DG proteome showed the most robust changes (Figures 7C and S7A; Table S4), which suggests EV-mediated Notch1 activation may play an important role in DG.[47] The Database for Annotation, Visualization and Integrated Discovery analysis of the downregulated proteins revealed a significant enrichment of the term "glutamatergic synapses" in the datasets from all three regions (top 2 in CA1, top 3 in CA3, top 7 in DG, Figure 7D; Table S4). Our finding is consistent with a recent study showing that *Alix*$^{-/-}$ hippocampal neurons have shorter postsynaptic densities and smaller spine head size compared to WT controls.[44] These data strongly suggest EV-mediated neural communication is required for normal glutamatergic synaptic protein expression in the hippocampus.

DISCUSSION

We discovered that activating synaptic NMDARs triggers hippocampal neurons to release Notch1 and Notch2 proteins in EVs. These EVs facilitate short-range, irreversible, cell-type-specific Notch signaling selectively in neurons. This EV-based Notch signaling pathway requires the ESCRT-associated protein Alix, and adult Alix cKO mice have reduced hippocampal Notch signaling. Thus, we discovered EVs mediate neuron-to-neuron communication, in which the Notch1 and Notch2 proteins play a neurotransmitter-like role, and the Notch ligands are the receptors for EV signaling.

Our results indicate Notch receptor-ligand binding facilitates EV capture on the neuronal plasma membrane and subsequent endocytosis.[2,4] In a similar way during canonical Notch signaling, Notch receptor-ligand complexes are endocytosed into acceptor cells.[18] Consistently, we found that in general most EVs have intact membranes after internalization (Figures 2C, 2E, and S3A). Endocytosis occurs at many locations spread across the neuronal plasma membrane, but glutamatergic presynaptic sites are particularly active sites of endocytosis.[22] Presynaptic Jag1 and Jag2 may regulated the EV uptake in axon terminals.[9,13] Interestingly, we also detected a small portion of the Jag1 and Jag2 pool in the PSD fraction (Figures S2B, S2C, and S2E). In contrast, synaptic Dll1 and Dll4 are exclusively detected within the postsynaptic compartment. Dendrites and spines are also endocytosis hotspots.[23,24] Therefore, postsynaptic Jag1, Jag2, Dll1, and Dll4 may contribute to the EV uptake in dendritic spines. Based on our hypothesis, after internalization, EVs are transported to the soma through retrograde trafficking.[50] Once activated, Notch$_{ICD}$ is proteolytically processed, enters the nucleus, and initiates Notch target gene expression. However, the mechanisms governing the translocation of EV-associated Notch receptors

into the nucleus remain unclear. We hypothesize two potential mechanisms. First, it could involve endosome-nucleus communication pathways.[51,52] Alternatively, it may be associated with the lysosome-to-nucleus signaling mechanism.[53–55] Further experiments will be needed to comprehensively investigate these mechanisms.

These findings linking the Notch signaling pathway to EVs provide an unconventional perspective on more than one hundred years of research on this evolutionarily conserved cell-to-cell communication pathway.[56,57] For example, in CNS neurons, Notch1 and Notch2 have been found to be expressed at dendritic spines, and Jag1 is mainly present at presynaptic sites.[28] Thus, in this arrangement, binding of the postsynaptic receptors and the presynaptic ligands in *trans* would result in endocytosis of the Notch receptor-ligand complex and constitutive activation of the Notch signaling pathway in the presynaptic neurons. However, in addition to the plasma membrane and cycling endosomes, Notch proteins also localize to intralumenal vesicles (ILVs) within MVBs. In hippocampal neurons, MVBs are mainly distributed in cell bodies and dendrites,[37] suggesting that the postsynaptic Notch proteins may be primarily localized to dendritic ILVs rather than to the dendritic spine plasma membrane. Notably, MVBs are important sites of EV biogenesis and storage, including exosomes,[3,5] and Notch proteins have been observed in MVBs that were previously thought to be en route to lysosomal degradation.[18] However, our results show that Notch-containing dendritic ILVs are also be secreted as EVs in an Alix-dependent manner in the mammalian neurons (Figure 4). Notably, many other parallel mechanisms exist for EV biosynthesis and release, including non-canonical ESCRT-dependent pathways and ESCRT-independent routes.[3,4] Notably, Alix is not essential for these EV biosynthesis or release pathways. In future studies, it is worth exploring the roles of these pathways in the generation of neuronal EVs induced by various stimuli.

In adult brain, Notch signaling activity contributes to synaptic plasticity, learning, and memory.[21,28,47,48,58] Furthermore, genetic inactivation of the Notch target gene *Hes1*expression in excitatory neurons resulted in abnormal fear and anxiety-related behavior in adult mice.[49] In the context of our findings, EV-based Notch signaling may underlie these observations in the adult brain. We found that *in vitro* EVs require at least 1 h to induce gene expression after stimulation of synaptic NMDARs (Figure 3B). Therefore, EVs are unlikely to regulate short-term synaptic plasticity and are more likely to play a key role in regulating long-term synaptic processes such as late-phase long-term potentiation and memory consolidation. Notably, since EVs also commonly contain nucleic acids (i.e., miRNA and mRNA), EV-based neuronal communication is likely to also regulate gene expression beyond Notch target genes. In summary, we discovered EVs facilitate cell-type-specific communication between neurons through the Notch ligand-receptor system.

Limitations of the study

While our discoveries regarding EV-mediated neuron-to-neuron communication are significant, there are several limitations to be acknowledged. First, we used a glycine solution lacking Mg^{2+} to activate synaptic NMDARs to initiate the release of EVs. However, it's important to note that this stimulation only partially replicates the complexities of excitatory synaptic activity in the brain. Given the diverse panel of neurotransmitters and

glutamate receptors in brain,[59] the *in vivo* conditions for EV release are likely more intricate than *in vitro*. Second, our understanding of EV abundance *in vivo* remains unclear. Therefore, we still do not know how important or widespread EV-based Notch signaling pathway activation is in the brain. Third, the synaptic architecture within the brain is notably more intricate compared to primary cultured neurons. For instance, glutamatergic synapses are partially enveloped by astrocytes.[60] Consequently, not all EVs released from dendritic spines can freely diffuse to distant areas. Furthermore, these EVs may even undergo internalization by astrocytes encasing the spines from which the EVs were released[61] and may involve distinct uptake mechanisms.[4] Each of these aspects may open alternative pathways for further investigation.

STAR★METHODS

RESOURCE AVAILABILITY

Lead contact—Further information and requests for resources and reagents should be directed to and will be fulfilled by the lead contact, Dr. Jeffrey N. Savas (jeffrey.savas@northwestern.edu).

Materials availability—We are glad to share plasmids generated in this study upon request.

Data and code availability

- The bulk RNA sequencing data presented in this study was deposited in Gene Expression Omnibus (GEO) under the identifier GSE110908. The mass spectrometry data presented in this study was deposited in Mass Spectrometry Interactive Virtual Enviroment (MassIVE) under the identifier MSV000093592 and ProteomeXchange under the identifier PXD047597. Other data reported in this study will be shared by the lead contact upon request.
- This paper does not report original code.
- Any additional information required to reanalyze the data reported in this work paper is available from the lead contact upon request

EXPERIMENTAL MODEL AND STUDY PARTICIPANT DETAILS

Animals—All procedures were approved by Northwestern University's Animal Care and Use Committee (IS00009900, IS00010858 and IS00001789) in compliance with US National Institutes of Health standards.

Mice: The $Alix^{+/-}$ mice (strain, C57BL/6) were generated by d'Azzo lab.[33] We bred these mice to obtain both $Alix^{-/-}$ and $Alix^{+/+}$ genotypes. The $Alix^{fl/fl}$ mice (strain, C57BL/6N) were generated by Sadoul lab.[39] The *Camk2a-Cre* mice were purchased from The Jackson Laboratory (B6.Cg-Tg(Camk2a-cre)T29–1Stl/J, Strain #:005359). We first crossed $Alix^{fl/fl}$ mice with homozygous *Camk2a-Cre* mice to generate *Camk2a-Cre::*$Alix^{fl/WT}$ mice, which were further used as breeders to generate *Camk2a-Cre::*$Alix^{fl/fl}$ mice. To examine the activation of the Notch signaling pathway, $Alix^{-/-}$ and $Alix^{+/+}$ mice at P0, P4, and P14

stages were employed. Around 2-month-old *Alix*$^{fl/fl}$ and *Camk2a-Cre::Alix*$^{fl/fl}$ mice were also used. *Alix*$^{+/+}$ mice of 2-to-3-month-old were used for subcellular fractionation. For TMT-MS, 2-to-3-month-old *Alix*$^{fl/fl}$ and *Camk2a-Cre::Alix*$^{fl/fl}$ mice were used. In all of the experiments, both male and female mice were used. All mice were maintained under a 12-h light/dark cycle and had continuous access to food and water.

Rat: Timed pregnant female Wistar rats were purchased from Charles River. All rats were maintained under a 12-h light/dark cycle and had continuous access to food and water. New born P0 pups (both male and female) were used for neuronal culture experiments.

Primary culture of hippocampal cells—Brains of postnatal day 0 Wistar rat or mouse pups were removed rapidly and placed in ice-cold Hank's Balanced Salt Solution (Thermo Fisher Scientific, Cat# 14170112). Hippocampi were dissected and incubated with papain for 20 min at 37°C, followed by trituration with fire-polished glass pipettes, and plated in poly-D-lysine (Fisher Scientific, Cat# CB-40210)/laminin (Fisher Scientific, Cat# 23-017-015) -coated 60-mm culture dishes (2×10^6 cells per dish), in 6-well plate (cover glasses, Carolina, Cat# 633037, 1.5×10^6 cells per well), in 12-well plate (5×10^5 cells per well), 24-well plates (cover glasses, Carolina, Cat# 633029, 1.5×10^5 cells per well). Notably, the *Alix*$^{+/-}$ mice were used as breeders. Therefore, mouse hippocampal neurons from each P0 pup were cultured individually. The tail of the corresponding mouse pup was used for the genotyping (Transnetyx). Neurons were cultured with Neurobasal medium supplemented with SM1 (STEMCELL Technologies, Cat# 05711) and maintained at 37°C in a humidified 5% CO_2 atmosphere incubator. Cultures were fed three times a week with changing 50% of the medium. Glial cell division was suppressed by addition of 5-fluoro-2-deoxyuridine (20 μg/mL; Sigma-Aldrich, Cat# F0503) and uridine (20 μg/mL; Sigma-Aldrich, Cat# U6381) at day four after plating (DIV 4). For EV enrichment, DIV 28 neurons were used. For immunostaining and WB, DIV 21–28 neurons were used. For electrophysiological recording and live cell imaging, DIV 15–18 neurons were used. For EV uptake experiments, glial cell division was not inhibited.

METHOD DETAILS

Plasmids and lentivirus (LV)—The mCherry-Alix plasmid and Notch1-myc were purchased from Addgene (Cat# 21504, and Cat# 41728). The pz196 plasmid was acquired from Dr. Evangelos Kiskinis lab. The GFP and mCheery plasmids were acquired from Dr. Peter Penzes lab. The mCherry-Alix-S717A and mCherry-Alix-S717D constructs were generated by QuikChange method with following oligoes[72]:

AlixS717A_For: acttgcaacaaGCAattgccagagaacctagtgct

AlixS717A_Rev: gttctctggcaatTGCttgttgcaagtcctttaag

AlixS717D_For: acttgcaacaaGATattgccagagaacctagtgct

AlixS717D_Rev: gttctctggcaatATCttgttgcaagtcctttaag

The mCherry, mCherry-Alix, mCherry-Alix-S717A and mCherry-Alix-S717D LVs were packaged by System Biosciences. The Notch1-myc lentiviruses (LV) were packaged in the Savas lab. LVs were added into primary cultured *Alix*$^{-/-}$ mouse or rat hippocampal neurons at DIV 4.

Electrophysiological recording—14–16 days after plating, coverslips were transferred to a recording chamber positioned under an upright microscope equipped with a 40× objective. They were continuously super fused (1 mL/min) with oxygenated sodium ACSF containing 125 mM NaCl, 2.4 mM KCl, 1.2 mM NaH_2PO_4, 25 mM $NaHCO_3$, 25 mM glucose, 2 mM $CaCl_2$, and 1mM $MgCl_2$ (pH 7.4; osmolarity between 325 and 335 mosmol-1) and maintained at near physiological temperature (32°C) on a heated stage. Whole-cell patch clamp recordings were performed using a Multiclamp700B amplifier (Axon Instruments Inc.). Borosilicate glass recording electrodes with resistances of 4–6 MΩ were filled with the following internal solution: 95 mM CsF, 25 mM CsCl, 10 mM Cs-HEPES, 10 mM Cs-EGTA, 2 mM NaCl, 2 mM Mg-ATP, 10 mM QX-314, 5 mM TEA-Cl, 5 mM 4-AP, (pH adjusted to 7.3 with CsOH). Series resistance was continuously monitored using hyperpolarizing voltage steps generated by pClamp 10.7 software (Axon Instruments), and recordings were discarded if there was a >15% change during the course of the experiment. No electronic compensation for series resistance was applied. Recordings were filtered at 2 kHz. All mEPSC recordings were made in the presence of TTX (0.5 μM) and GABAA receptor antagonists, picrotoxin (50 μM) and bicuculline (10 μM). For cLTP induction, perfusion was switched for 5 min to a Magnesium-free ACSF containing Glycine (200μM). mEPSC were analyzed using miniAnalysis (Bluecell) with a threshold set at 5 pA.

Neuronal EV release induction—We activated synaptic NMDARs using a glycine-based manner.[16,73] Neurons were washed three times with warm Mg^{2+}-free glycine solution (pH 7.4, 150 mM NaCl, 5 mM KCl, 200 mM glycine, 2 mM $CaCl_2$, 10 mM glucose, 10 mM HEPES, 1 μM Strychnine, 20 μM Bicuculline. The osmolarity was adjusted to 300–330 mOsm/l). The neurons were kept in Mg^{2+}-free glycine solution for 30 min at 37°C in a humidified 5% CO_2 atmosphere incubator. The EV-containing supernatant was then carefully collected to enrich for EVs. As a negative control experiment, we did a treatment of neurons with the Veh solution (pH 7.4, 150 mM NaCl, 5 mM KCl, 1 mM $MgCl_2$, 2 mM $CaCl_2$, 10 mM glucose, 10 mM HEPES, 1 μM Strychnine, 20 μM Bicuculline. The osmolarity was adjusted to 300–330 mOsm/l). The Veh solution with which the neurons had been treated was also collected for further analysis.

SEC-based EV enrichment—The EV-containing supernatant was centrifuged at 3000 × g for 30 min at 4°C to remove residual neurons and large debris. Then, the supernatant was concentrated using a molecular weight cutoff (MWCO) filter (10 kDa, EMD Millipore, Cat# UFC801024) to ~0.5 mL. The concentrated solution was then fractionated into 10 fractions (0.5 mL in EV-free PBS, MEDIATECH INC CA, Cat# 21–040-CV) using a qE-Voriginal-35nm SEC column (Izon Science, Cat# SP5-USD) with an automated fraction collector V1 (Izon Science, Cat# AFC-V1).

Quantification of EV size—Purified EV samples were submitted to Center for Advanced Microscopy/Nikon Imaging Center (Northwestern University) for negative staining EM analysis. Images were acquired with a FEI Tecnai Spirit G2 120 kV transmission EM. EM images were imported into Fiji (NIH, https://imagej.nih.gov/ij/). All visible EV-like particles were measured and no particles were omitted. Before measurement, the images were processed with sharpen function for edge-detection.

Quantification of EV—For each experimental group, EVs released from three 60 mm dishes of mouse hippocampal neurons were pooled and enriched by the SEC method as described above. Then take 10 μL of the enriched EVs from each sample and dilute them with 990 μL EV-free PBS. The samples were centrifuged at 2500 × g for 15 min. Mix 0.5 mL of each sample with 0.5 mL incubation solution. Load 70 μL of each mixture to an ExoView Mouse Tetraspanin chip (Nanoview Bioscience, Cat# EV-TETRA-M2) and incubate overnight at RT in dark. The next day, unbound EVs were washed off the chip by five 3-min washes with the solution A. After incubating with the block solution for 1 h (RT), the chips were incubated with anti-tetraspanin mixture (Included in the kit, anti-CD81, CF 555, anti-CD9, CF 488A and anti-CD63, CF 647) for 1 h on an orbital shaker. The chips were washed with the solution A twice (3 min each) and the solution B 5 times (3 min each). The chips were then rinsed in MilliQ water to remove excess solution B. Air dry the chips. A NanoView R100 equipment (Nanoview Bioscience) was used to scan the chips. The data was analyzed by ExoView Analyzer 3.1.4 (Nanoview Bioscience).

EV labeling—EVs were labeled with the protein dye CFSE or the lipid dye CM-Dil.[74] EV-containing solution was collected from twelve 60 mm culture dishes (DIV 28, 2×10^6 cells per dish) as described above. The solution was then concentrated to ~0.5 mL using a 10 kDa MWCO filter. CFSE (Thermo Fisher Scientific, Cat# C34554) and CM-Dil (Thermo Fisher Scientific, Cat# C7000) dyes were resuspended with DMSO (Sigma-Aldrich, Cat# D2650) and adjusted to 5 mM and 7.5 μM respectively. 8 μL CFSE or 10 μL CM-Dil was added to each 0.5 mL of concentrated EV-containing solution. The mixture was incubated for 1 h in the dark in a 37°C water bath. Then, as described above, we enriched labeled EVs and removed excess dyes by SEC fractionation (as above). Labeled EVs exist in SEC F2, which was concentrated to ~20 μL using an MWCO filter (30 kDa, Millipore Sigma, Cat# MRCF0R030).

Proteinase K (PK) treatment of EV—EV-containing solution was collected from twelve 60 mm culture dishes (DIV 28, 2×10^6 cells per dish) as described above. The solution was then concentrated to ~0.5 mL using a 10 kDa MWCO filter and divided into two equal parts (~0.25 mL each). PK (Fisher Scientific, Cat# NC0547027) was added into one part and made final concentration to 100 μg/mL. Both parts were incubated for 1 h in the dark in a 37°C water bath. Then deactivate PK by heating at 95°C for 10 min. Volume each part to 0.5 mL with PBS. Then, label the EVs with CFSE dye, and enrich the labeled EVs by SEC fractionation as shown above. The volume of each part was reduced to ~20 μL using a 30 kDa MWCO filter.

Dleta^{MAX} treatment of EV—EVs were collected from twelve 60 mm culture dishes (DIV 28, 2 × 10^6 cells per dish) as described above. The solution was then concentrated to ~0.5 mL using a 10 kDa MWCO filter and divided into two equal parts (~0.25 mL each). Delta^{MAX} was added into one part and made final concentration to 5 μM. Both parts were incubated for 30 min in the dark with rotation at 4°C. Then the volume was brought up to 0.5 mL total with PBS. Then, the EVs were enriched by SEC fractionation as described above. The volume of each tube was reduced to ~20 μL using a 30 kDa MWCO filter.

Neuronal EV uptake assay—The labeled EVs were diluted with 300 μL neuronal culture medium and divided into three equal portions. 100 μL of diluted labeled EVs were added into one well of a 24-well plate of primary cultured hippocampal neurons (DIV 21–28, on cover glasses, 1.5 × 10^6 cells per well). The plate was incubated at 37°C in a humidified 5% CO_2 atmosphere incubator for 30 min. Then wash three times in D-PBS (Fisher Scientific, Cat# AAJ67802K2) to remove non-absorbed EVs. After being fixed with 4% PFA (in D-PBS, 4% sucrose) for 15 min at RT with gentle agitation, immunocytochemistry was performed on the samples.

Lactate dehydrogenase (LDH) assay—After collection of the culture medium, the neurons were treated with either Vehicle (Veh) or Mg^{2+}-free glycine solution for 30 min at 37°C in a humidified 5% CO_2 atmosphere incubator. An LDH assay kit (Thermo Fisher Scientific, Cat# 88953) was then used to measure LDH levels in the culture medium, Veh, or Mg2+-free glycine solution with which the neurons were treated. An aliquot of each sample (100 μL) was transferred from the culture wells to the wells of a 96-well plate and mixed with 100 μL of the reaction solution provided by the kit. Optical density was measured at 492 nm 45 min later using a Synergy HTX multi-mode microplate reader (Biotek). Background absorbance at 620 nm was subtracted. The maximal releasable LDH in each well was then obtained by a 15 min incubation with 1% Triton X-100 at the end of each experiment.

Live cell imaging—DIV 18 rat hippocampal neurons in 6-well plate (cover glasses, Carolina, Cat# 633037, 1.5 × 10^6 cells per well) were used for this assay. At DIV 16, neurons were co-transfected with either 1 μg mCherry + GFP or 1 μg mCherry-Alix + GFP plasmids using HilyMax (Dojindo, Cat# H357–15). Two days later, the neurons were used for live cell imaging analysis. Neurons (put in a magnetic imaging chamber, Warner Instruments, Cat# QR-40L) were rinsed three times with warm (37°C) extracellular solution (pH 7.4, 150 mM NaCl, 5 mM KCl, 1 mM $MgCl_2$, 2 mM $CaCl_2$, 10 mM glucose, 10 mM HEPES). Then the neurons were placed into a heating stage (37°C) supplied with a humidified 5% CO_2 atmosphere and were incubated with this solution for 20 min in a humidified 5% CO_2 atmosphere incubator at 37°C. After washing twice with warm Mg^{2+}-free glycine solution, the neurons were incubated with Mg^{2+}-free glycine solution for 5 min. Then the extracellular solution was put back. Images were captured using a Nikon A1R + confocal laser microscope and a 100× oil objective lens (also was kept at 37°C during recording). To minimize bleaching, we only sampled the signals at indicated time points in Figure S1. The data was imported to Fiji (NIH) for further analysis.[73]

Immunocytochemistry (ICC)—Neurons (cultured on cover glasses) were washed three times with D-PBS (Fisher Scientific, Cat# AAJ67802K2). Neurons were then fixed with 4% PFA (in D-PBS, 4% sucrose) for 15 min at RT with gentle agitation. PFA was quenched by three 5-min washes in PBS (1 M glycine). Three subsequent 5-min washes with PBS removed glycine. After blocking (10% horse serum, 0.1% Triton X-100 in PBS) for 1 h, neurons were incubated with primary antibodies overnight at 4°C with gentle agitation. Following primary antibodies were used: chicken anti-MAP2 (1:5000, Millipore Sigma, Cat#AB5543, RRID: AB_571049), mouse anti-Jag1 (1:1000, Santa Cruz Biotechnology, Cat# sc-390177, RRID: AB_2892141), goat anti-Jag2 (1:1000, Thermo Fisher Scientific, Cat# PA5–47188, RRID: AB_2576459), rabbit anti-Jag2 (1:1000, Cell Signaling Technology, Cat# 2210, RRID: AB_823553), goat anti-Dll1 (1:1000, Abcam, Cat# ab85346, RRID: AB_1860332), rabbit anti-Dll1 (1:1000, Cell Signaling Technology, Cat#2588, RRID: AB_2292961), goat anti-Dll4 (1:1000, Thermo Fisher Scientific, Cat# PA5–46974, RRID: AB_2577158), rabbit anti-Dll4 (1:1000, Cell Signaling Technology, Cat# 96406, RRID: AB_2800263), guinea pig anti-VGluT1 (1:1000, Millipore Sigma, Cat# AB5905, RRID: AB_2301751), rabbit anti-Homer1 (1:1000, Synaptic Systems, Cat# 160 003, RRID: AB_887730), mouse anti-Tsg101 (1:1000, Santa Cruz Biotechnology, Cat# sc-7964, RRID: AB_671392), rabbit anti-Notch1$_{ICD}$ (1:1000, Abcam, Cat# ab52627, RRID: AB_881725), mouse anti-LBPA (1:500, Millipore Sigma, Cat # MABT837), rabbit anti-Notch2$_{ICD}$ (1:1000, Cell Signaling Technology, Cat# 5732S, RRID: AB_10693319), mouse anti-PSD95 (1:500, Thermo Fisher Scientific, Cat # MA1–046, RRID: AB_2092361), chicken anti-GFP (1:5000, Abcam, Cat# ab13970, RRID: AB_300798) and mouse anti-myc (1:1000, Santa Cruz Biotechnology, Cat# sc-40, RRID: AB_627268). After six 5-min-washes in PBS, neurons were incubated with corresponding Alexa Fluor secondary antibodies (1:1000, Thermo Scientific, Cat# A11057, A11034, A10037, A-11011, A11029, A11055, A-21437 and Abcam Cat# ab150187) overnight at 4°C with mild agitation. Then, after six 5-min-washes in PBS, neurons were incubated in 4′,6-diamidino-2-phenylindole (1:1000, DAPI, Sigma-Aldrich, Cat# D9542) solution for 5 min. Neurons were washed one more time with PBS and mounted with Fluoromount-G (Southern Biotech, Ca # 0100–01) on microscope slides.

Images were captured using a Nikon A1R + confocal laser microscope and 20 × or 100× objective lens. For each coverslip, area was randomly selected. Images were processed and analyzed by Fiji (NIH) with plugins Ratioplus, Colocalization Finder, and JACOP. Imaris (Oxford Instruments) 10.0.0 was used for spine analysis.

Using EVs to treat neurons—PK-related experiments: enriched EVs from twelve 60 mm culture dishes (DIV 28, 2 × 10^6 cells per dish) were divided into two equal parts. One part of EVs were treated with PK as mentioned above. SEC fractionation was used to remove excess PK. Veh (20 μL PBS), EVs (20 μm) and PK-treated EVs (20 μL) were each added to three wells of cultured neurons in an 8-well plate, respectively.

Delta^{MAX}-related experiments: enriched EVs from twelve 60 mm culture dishes (DIV 28, 2 × 10^6 cells per dish) were divided into two equal parts. One-half of the EVs were treated with Delta^{MAX} as mentioned above. SEC fractionation was used to remove excess Delta^{MAX}. Veh (20 μL PBS), EVs (20 μm), Delta^{MAX} -treated EVs (20 μL) and Delta^{MAX}

(5 μM in 20 μL PBS) were each added to four wells of cultured neurons in an 8-well plate, respectively.

The plates were incubated at 37°C in a humidified 5% CO_2 atmosphere incubator for 1hr. The neurons were harvested for WB analysis.

Pharmacological treatments of neurons—Neurons were pretreated with DMSO (1:1000) or dynasore (80 μM, Sigma-Aldrich, Cat# SML0340) or H89 (20 μM, Sigma-Aldrich, Cat# B1427) or staurosporine (1 μM, Tocris, Cat# 1285) or APV (50 μM, Sigma-Aldrich, Cat# A5282) or KN93 (10 μM, Sigma-Aldrich, Cat# K1385) or AIP (1 μM, Anaspec, Cat# AS-64929) for 30 min at 37°C in a humidified 5% CO_2 atmosphere incubator. Then, neuron culture medium was carefully removed from dishes. The collected medium was then kept at 37°C in a humidified 5% CO_2 atmosphere incubator. The neurons were washed three times with Veh or Mg^{2+}-free glycine and incubated for 5 min with solutions containing different inhibitors. Then neurons were washed twice with Veh solution, the saved culture medium was returned and maintained in incubator for assigned durations (37°C, 5% CO_2).

Poly-A RNA sequencing—Total RNA was extracted from neurons using RNeasy mini Kit (Qiagen, Cat# 74104). Ribosomal RNA was depleted with RiboZero kit (Epicentre, Cat# MRZH116). Poly(A)-enriched RNA were separated by three rounds of Oligo(dT) magnetic beads (Thermo, Cat# 61002). For each time point, RNA from two 60-mm dishes of neurons were pooled together. Sequence quality was assessed using FastQC, and quality trimming was done using Trimmomatic.[69] RNA-seq reads were aligned to the rat genome (iGenomes UCSC version rn6) using TopHat v2.0.9, and only uniquely mapped reads with at most two mismatches were considered for downstream analysis. Gene count tables were constructed using HTseq[70] and used as input for edgeR 3.0.8 [71]. The list of activity regulated genes is generated based on previous *in vivo* studies.[75–77]

Subcellular fractionation—Adult mouse cortexes were rinsed and dissected in solution A (5 mM HEPES pH 7.4, 1 mM $MgCl_2$, 0.5 mM $CaCl_2$, 1 mM DTT, 0.32 M sucrose and protease and phosphatase inhibitor set (Thermo Fisher Scientific, Cat#: 78443_3670527377)) on ice. Then the tissues were homogenized with an electronic homogenizer (Glas-Col, Cat# 099C-K54). Spin down the homogenates at 1,400 × g for 10 min (4°C). Set aside the supernatant. Then we resuspended the pellets in 20 mL solution A. The diluted homogenates were centrifuged at 710 × g for 10 min (4°C). The pellet is P1. We combined and mixed the supernatant and the saved supernatant as S1.

S1 were centrifuged at 13,800 × g for 10 min (4°C). The supernatant is S2. Then we resuspended the pellets (P2) in solution B (6 mM Tris pH 8.1, 0.32 M sucrose, 1 mM EDTA, 1 mM EGTA, 1 mM DTT with protease and phosphatase inhibitors). Then we layered the homogenized pellets on discontinuous sucrose gradient (1.2 M. 1.0 M and 0.85 M sucrose in 6 mM Tris pH 8.1) and centrifuged it at 82,000 × g for 2 h (4°C). Collect the layer between the 1.0 M and 1.2 M interface and dilute it in 2.5 × volume with 6 mM Tris pH 8.1. Then centrifuge it at 200,000 × g for 30 min (4°C). The pellet is synaptosome (SS). Then SS were incubated in ice-cold solution C (50 mM HEPES pH 8.1, 2 mM EDTA, 0.5% Triton

X-) for 15 min rotation in 4°C and then centrifuged at 32,000 × g for 20 min (4°C). The supernatant is presynaptic fraction (Pre). The pellet is resuspended in in ice-cold solution C for 15 min one more time and then centrifuged at 32,000 × g for 20 min (4°C). The pellet is postsynaptic density (PSD) fraction. BCA (Thermo Fisher Scientific, Cat# 23225) all the fraction.

Western blotting (WB)—Each SEC fraction was further concentrated to ~40 μL using an MWCO filter (30 kDa, Millipore Sigma, Cat# MRCF0R030). An equal volume of 2 × SDS loading buffer was then added to the sample and mixed. The mixture was heated at 95°C for 5 min. Each SEC fraction sample was divided into two equal parts for WB and silver staining analyses.

Neuron samples were collected and resuspended in a RIPA lysis buffer (50 mM Tris, 150 mM NaCl, 0.1% SDS, 1mM EDTA, 0.5% sodium deoxycholate, 1% Triton X-100, 1 × protease inhibitor cocktail (Thermo Fisher Scientific, Cat# 78443), 1 × phosphatase inhibitor (Thermo Fisher Scientific, Cat# 78420), pH 7.4). The resuspended lysates were vortexed for 20 s and then incubated on ice for 30 min and centrifuged at 16,200 g for 15 mins. The supernatants were mixed with 4 × SDS loading buffer at a 3:1 ratio. The mixtures were boiled at 95°C for 5 min.

Dissected mouse hippocampi were homogenized in RIPA lysis buffer (50 mM Tris, 150 mM NaCl, 0.1% SDS, 1mM EDTA, 0.5% sodium deoxycholate, 1% Triton X-100, 1 × protease inhibitor cocktail (Thermo Fisher Scientific, Cat# 78443), 1 × phosphatase inhibitor (Thermo Fisher Scientific, Cat# 78420), pH 7.4) with an electronic homogenizer (Glas-Col, Cat# 099C-K54). The resuspended lysates were vortexed for 20 s and then incubated on ice for 30 min and centrifuged at 16,200 g for 15 mins. Samples were further cleaned up by methanol chloroform precipitation. The protein pellets were resuspended in 1 × SDS loading buffer and boiled at 95°C for 5 min.

WedgeWell Tris-Glycine Mini Protein Gels (Fisher Scientific, Cat# XP04125BOX, XP04120BOX and XV00100PK20) were used for electrophoresis. After electrophoresis, proteins were transferred onto nitrocellulose membranes (Thermo Fisher, Cat# 4500002). For WB, the membranes were blocked with 10% bovine serum albumin (BSA, Jackson immunoResearch laboratories, Cat# 001–000-162) in TBST solution (Tris-buffered saline, 0.1% Tween 20) for 1 h in room temperature (RT). Then membranes were incubated with primary antibodies in incubation solution (3% BSA in TBST) overnight at 4°C with mild agitation. Following primary antibodies were used: mouse anti-Alix (1:1000, Cell Signaling Technology, Cat# 2171S, RRID: AB_2299455), rabbit anti-Alix (1:1000, Cell Signaling Technology, Cat# 18269, RRID: AB_2798796), mouse anti-Tsg101 (1:1000, Santa Cruz Biotechnology, Cat# sc-7964, RRID: AB_671392), mouse anti-CD81 (1:1000, Santa Cruz Biotechnology, Cat# sc-166029, RRID: AB_2275892), rabbit anti-Notch1-$_{ICD}$ (1:1000, Abcam, Cat# ab52627, RRID: AB_881725), rabbit anti-Notch2$_{ICD}$ (1:1000, Cell Signaling Technology, Cat# 5732S, RRID: AB_10693319), rabbit anti-activated Notch1 (1:1000, Abcam, Cat# ab52301, RRID: AB_881726), rabbit anti-activated Notch2 (1:1000, MyBioSource, Cat# MBS9410510), rabbit anti-Sdcbp (1:1000, Abcam, Cat# ab19903, RRID: AB_445200 and Cell Signaling Technology, Cat # 27964), rabbit anti-GM130

(1:1000, Abcam, Cat# ab52649, RRID: AB_880266), rabbit anti-Hes1 (1:1000, Cell Signaling Technology, Cat# 11988S, RRID: AB_2728766 and Abcam, Cat# ab71559, RRID: AB_1209570), chicken anti-Tuj1 (1:2000, Novus Biologicals, Cat#NB100–1612, RRID: AB_10000548), rabbit anti-p-S/T (1:1000, Cell Signaling Technology, Cat# 9624S, RRID: AB_331817), mouse anti-PSD95 (1:2000, Thermo Fisher Scientific, Cat# MA1–046, RRID: AB_2092361), rabbit anti-PSD95(pS295) (1:1000, Abcam, Cat# ab76108, RRID: AB_1310621), rabbit anti-GAPDH (1:2000, Cell Signaling Technology, Cat# 2118, RRID: AB_561053), rabbit anti-GluA1 (1:1000, EMD Millipore, Cat# PC246, RRID: AB_564636) and guinea pig anti-Bassoon (1:1000, Synaptic Systems, Cat# 141 318, RRID: AB_2927388). After 3 × 10 min intense wash in TBST solution, membranes were incubated with corresponding secondary antibodies for 1 h at RT with mild agitation. Following secondary antibodies were used: goat-*anti*-rabbit poly-HRP (1:2000, Thermo Scientific, Cat# 32260), goat-*anti*-mouse poly-HRP (1:2000, Thermo Scientific, Cat# 32230), goat-*anti*-chicken HRP (1:2000, Abcam, Cat# ab97135) and Goat anti-Guinea Pig poly-HRP (1:2000, Fisher Scientific, Cat# OB6090–05). Then membranes were washed 3 × 10 min in TBST and developed with SuperSignal West Pico Chemiluminescent Substrate (Thermo Fisher, Cat# 34578) and imaged on a Chemidoc XRS system (Bio-Rad). Fiji (NIH) was used for quantification.

Immunoprecipitation (IP)—Three-five 60 mm-dishes of primary cultured rat hippocampal neurons were collected and re-suspended in IP buffer (20 mM Tris-Cl, pH 7.4, 150 mM NaCl, 1% Triton X-100, 1 mM EDTA, 3 mM NaF, 1 mM β-glycerophosphate, 1 mM sodium orthovanadate, 2 mM N-ethylmaleimide and 10% glycerol) with complete protease and phosphatase inhibitor set (Thermo Fisher, Cat# 78443). After incubating on ice for 30 min, the lysates were centrifuged at 13,000 × g for 15 min (4°C). Supernatant were collected and precleared with 100 μL Protein G Sepharose 4 Fast Flow (Thermo Fisher, Cat# 45–000-116) for 1 h at 4°C. Then samples were incubated with two μg mouse anti-Alix (Cell Signaling Technology, Cat# 2171) or IgG (Sigma-Aldrich, Cat# 15381) overnight at 4°C. The next day, 50 μL Protein G Sepharose 4 Fast Flow were added to the samples and incubated for 2 h at 4°C. Then, the beads were washed three times with IP buffer. The immunoprecipitants were eluted with 2 × SDS loading buffer.

Lambda phosphatase assay—Alix immunoprecipitates from neurons treated with Veh or Mg^{2+}-free glycine solution were resuspended in lambda phosphatase assay buffer (50 mM Tris-HCl pH 7.8, 5 mM dithiothreitol, 2 mM $MnCl_2$, 100 μg/mL BSA) with or without 1600 U of lambda phosphatase (New England Biolabs, Cat# P0753S). After 60 min at 30°C, the reactions were stopped by adding 2 × SDS loading buffer and processed for WB with the indicated antibodies.

Silver staining—We used Pierce Silver Stain Kit (Thermo Fisher, Cat# 24612) for silver staining. Gels were washed 2 × 5 min in ultrapure water and then fixed with 2 × 15 min in 30% ethanol: 10% acetic acid solution. Then the fixed gels were washed 2 × 5 min with 10% ethanol and 2 × 5 min in ultrapure water. Then the gels were sensitized for 1 min and washed twice 2 × 1 min with water. Then, the gels were stained for 30 min and washed 2 × 20 s with ultrapure water. The gels were developed for 1–3 min until bands appear and

stopped with 5% acetic acid for 10 min. A Chemidoc XRS system (Bio-Rad) was used for imaging.

Immunohistochemistry (IHC) staining—Mice were anesthetized and transcardially perfused with ice old PBS followed by 4% PFA (in PBS, pH 7.4). Dissected brains were cryoprotected in 30% sucrose solution and then buried in embedding medium (Sakura, Cat# 4583). Sagittal sections (35 μm) were obtained using a cryostat microtome. Slices were washed 3 × 5 min in glycine solution (1M glycine in PBS, pH 7.4) to block unreacted PFA. Slices were further washed 3 × 5 min in PBS to remove glycine. For permeabilization, slices were incubated in Triton X-100 (0.5% in PBS, pH7.4) solution for 1 h at RT. After blocking (10% horse serum, 0.5% Trition X-100 in PBS, pH7.4) for 1 h, slides were incubated with primary antibodies at 4°C for 48 h with mild agitation. Following primary antibodies were used: rabbit anti-Notch1$_{ICD}$ (1:500, Abcam, Cat# ab52627), rabbit anti-Notch2$_{ICD}$ (1:500, Cell Signaling Technology, Cat# 5732S) and chicken anti-Tuj1 (1:500, Novus Biologicals, Cat#NB100–1612). After 9 × 5 min washing in PBS, slides were incubated with corresponding Alexa Fluor secondary antibodies (1:1000, Thermo Scientific, Cat# A11034 and Abcam, Cat# ab150187) overnight at 4°C with mild agitation. Then, after 8 × 5 min washing in PBS, slides were incubated in 4′,6-diamidino-2-phenylindole (1:1000, DAPI, Sigma-Aldrich, Cat# D9542) solution for 10 min. The slides were washed 5 min with PBS and mounted with ProLong Diamond Antifade Mountant (Thermo Fisher Scientific, Cat# P36970) on microscope slides.

Images were captured using a Nikon A1R + confocal laser microscope and 100× objective lens. For each mouse, brain slices were randomly selected. Images were processed and analyzed by Fiji (NIH).

Sample preparation or MS analysis—Trichloroacetic acid (TCA, Sigma-Aldrich, Cat# T0699) precipitation was used to clean and precipitate proteins from SEC fractionation samples. Proteins from neuron samples and mouse hippocampal samples were extracted and precipitated as described in Western blotting (WB) section. Protein pellets were resuspended in 8 M urea (Thermo Fisher Scientific, Cat# 29700) prepared in 100 mM ammonium bicarbonate solution (Fluka, Cat# 09830). Dithiothreitol (DTT, DOT Scientific Inc, Cat# DSD11000) was applied to a final concentration of 5 mM. After incubation at RT for 20 min, iodoacetamide (IAA, Sigma-Aldrich, Cat# I1149) was added to a final concentration of 15 mM and incubated for 20 min at RT in the dark. Excess IAA was quenched with DTT for 15 min. Samples were diluted with 100 mM ammonium bicarbonate solution, and digested for 3 h with Lys-C protease (1:100, Thermo Fisher Scientific, Cat# 90307_3668048707) at 37°C. Trypsin (1:100, Promega, Cat# V5280) was then added for overnight incubation at 37°C with intensive agitation (1000 rpm). The next day, reaction was quenched by adding 1% trifluoroacetic acid (TFA, Fisher Scientific, Cat# O4902–100). The SEC fraction samples were desalted using ZipTip (Thermo Fisher–Pierce, Cat# 87784). The neuron and hippocampal samples were desalted using Peptide Desalting Spin Columns (Thermo Fisher Scientific, Cat# 89852). All samples were vacuum centrifuged to dry.

Enrichment of phosphorylated peptides—Neurons were stimulated with Mg^{2+}-free glycine solution for 10 min. Peptides were prepared as described above. The High-Select

TiO_2 Phosphopeptide Enrichment Kit (Thermo Fisher Scientific, Cat# A32993) was used to enrich phosphorylated peptides following the manufacturer's specifications.

Tandem Mass Tag (TMT) labeling—Our protocol was based on previously reported methods.[78] C18 column-desalted peptides were resuspended with 100 mM HEPES pH 8.5 and the concentrations were measured by micro BCA kit (Fisher Scientific, Cat# PI23235). For each sample, 100 μg of peptide labeled with TMT reagent (0.4 mg, dissolved in 40 μL anhydrous acetonitrile, Thermo Fisher Scientific, Cat# A44520) and made at a final concentration of 30% (v/v) acetonitrile (ACN). Following incubation at RT for 2 h with agitation, hydroxylamine (to a final concentration of 0.3% (v/v)) was added to quench the reaction for 15 min. TMT-tagged samples were mixed at a 1:1:1:1:1:1:1:1 ratio. Combined sample was vacuum centrifuged to dryness, resuspended, and subjected to HyperSep C18 Cartridges (ThermoFisher Scientific, Cat# 60108–302).

Peptide fractionation—We used a high pH reverse-phase peptide fractionation kit (Thermo Fisher Scientific, Cat# 84868) to get eight fractions (5.0%, 10.0%, 12.5%, 15.0%, 17.5%, 20.0%, 22.5%, 25.0% and 50% of ACN in 0.1% triethylamine solution). The high pH peptide fractions were directly loaded into the autosampler for MS analysis without further desalting.

Tandem mass spectrometry—Three micrograms of each fraction or sample were auto-sampler loaded with an UltiMate 3000 HPLC pump onto a vented Acclaim Pepmap 100, 75 μm × 2 cm, nanoViper trap column (Thermo Fisher Scientific, Cat# 164535) coupled to a nanoViper analytical column (Thermo Fisher Scientific, Cat# 164570, 3 μm, 100 Å, C18, 0.075 mm, 500 mm) with stainless steel emitter tip assembled on the Nano-spray Flex Ion Source with a spray voltage of 2000 V. An Orbitrap Fusion (Thermo Fisher Scientific) was used to acquire all the MS spectral data. Buffer A contained 94.785% H_2O with 5% ACN and 0.125% FA, and buffer B contained 99.875% ACN with 0.125% FA. For TMT-MS experiments, the chromatographic run was for 4 h in total with the following profile: 0–7% for 7, 10% for 6, 25% for 160, 33% for 40, 50% for 7, 95% for 5 and again 95% for 15 min receptively. For other MS experiments, the chromatographic run was for 2 h in total with the following profile: 2–8% for 6, 8–24% for 64, 24–36% for 20, 36–55% for 10, 55–95% for 10, 95% for 10 min.

We used a multiNotch MS^3-based TMT method to analyze all the TMT samples.[78–80] The scan sequence began with an MS^1 spectrum (Orbitrap analysis, resolution 120,000, 400–1400 Th, AGC target 2×10^5, maximum injection time 200 ms). MS^2 analysis, 'Top speed' (2 s), Collision-induced dissociation (CID, quadrupole ion trap analysis, AGC 4×10^3, NCE 35, maximum injection time 150 ms). MS^3 analysis, top ten precursors, fragmented by HCD prior to Orbitrap analysis (NCE 55, max AGC 5×10^4, maximum injection time 250 ms, isolation specificity 0.5 Th, resolution 60,000).

We used CID-MS^2 method for other experiments. Briefly, ion transfer tube temp = 300°C, Easy-IC internal mass calibration, default charge state = 2 and cycle time = 3 s. Detector type set to Orbitrap, with 60K resolution, with wide quad isolation, mass range = normal, scan range = 300–1500 m/z, max injection time = 50 ms, AGC target = 200,000, microscans

= 1, S-lens RF level = 60, without source fragmentation, and datatype = positive and centroid. MIPS was set as on, included charge states = 2–6 (reject unassigned). Dynamic exclusion enabled with n = 1 for 30 s and 45 s exclusion duration at 10 ppm for high and low. Precursor selection decision = most intense, top 20, isolation window = 1.6, scan range = auto normal, first mass = 110, collision energy 30%, CID, Detector type = ion trap, OT resolution = 30K, IT scan rate = rapid, max injection time = 75 ms, AGC target = 10,000, Q = 0.25, inject ions for all available parallelizable time.

MS data analysis and quantification—Protein identification/quantification and analysis were performed with Integrated Proteomics Pipeline - IP2 (Bruker, Madison, WI. http://www.integratedproteomics.com) using ProLuCID,[66,67] DTASelect2,[81,82] Census and Quantitative Analysis (For TMT-MS experiments). Spectrum raw files were extracted into MS1, MS2 and MS3 (For TMT experiments) files using RawConverter (http://fields.scripps.edu/downloads.php). The tandem mass spectra were searched against UniProt mouse (downloaded on 10–26-2020) or rat (downloaded on 03–25-2014) protein databases[83] and matched to sequences using the ProLuCID/SEQUEST algorithm (ProLuCID version 3.1) with 5 ppm peptide mass tolerance for precursor ions and 600 ppm for fragment ions. The search space included all fully and half-tryptic peptide candidates within the mass tolerance window with no-miscleavage constraint, assembled, and filtered with DTASelect2 through IP2. To estimate peptide probabilities and false-discovery rates (FDR) accurately, we used a target/decoy database containing the reversed sequences of all the proteins appended to the target database.[83] Each protein identified was required to have a minimum of one peptide of minimal length of six amino acid residues; however, this peptide had to be an excellent match with an FDR <1% (<5% for TiO_2 column-enriched samples) and at least one excellent peptide match. After the peptide/spectrum matches were filtered, we estimated that the peptide FDRs were ≤1% for each sample analysis. Resulting protein lists include subset proteins to allow for consideration of all possible protein forms implicated by at least two given peptides identified from the complex protein mixtures. Then, we used Census and Quantitative Analysis in IP2 for protein quantification of TMT-MS experiments and protein quantification was determined by summing all TMT report ion counts. For SEC samples, static modification: 57.02146 C for carbamidomethylation; differential modifications: 15.9949 M for oxidation on M. For neuron samples to detect phosphorylated peptides: static modification: 57.02146 C for carbamidomethylation; differential modifications: 15.9949 M for oxidation on M, 79.9663 STY for phosphorylation on S or T or Y residues. For TMT experiments: static modification: 57.02146 C for carbamidomethylation, 304.2071 for 16-plex TMT tagging; differential modifications: 15.9949 M for oxidation on M, 304.2071 for N-terminal 16-plex TMT tagging, 42.0106 for N-terminal Acetylation. More than one proteoform may be encoded by a single gene.[84] To minimize recalculation of the same peptides into multiple proteoforms, we grouped the peptides encoded by the same gene. The peptides are quantified and analyzed together.

Determination of EV proteins—To determine whether each protein was a true EV protein or a contaminant, we examined the distribution of each protein across all SEC fractions. True EV proteins must meet the following three criteria.

1. Compared to all other fractions, SEC F2 has significantly higher number of spec counts.
2. At least detected in two biological replicates in SEC F2.
3. Should not be detected in SEC F7–10. These fractions contain only small size particles such as protein aggregates and lipid droplets, which are much smaller than EVs.

QUANTIFICATION AND STATISTICAL ANALYSIS

Spyder (MIT, Python 3.7, libraries, ‘pandas’, ‘numpy’, ‘scipy’, ‘statsmodels’ and ‘bioinfokit’) was used for data statistical analyses. RStudio (version, 1.2.1335, packages, ‘tidyverse’, ‘pheatmap’) was used for data virtualization. The Database for Annotation, Visualization and Integrated Discovery (DAVID) was used for protein functional annotation analysis.[63,64] COBALT was used to run the alignment.[65] NCBI Multiple Sequence Alignment Viewer (Version 1.15.0) was used for alignment virtualization. We did not use specific methods to confirm whether the data met the required criteria for our selected statistical techniques. Rather, we chose these techniques based on their common usage in previous studies within our field and their general acceptance in comparable experiments. Statistical significance was established through appropriate statistical tests, for WB, ICC, IHC, bulk RNA-Seq and NanoView experiments, one-tailed Student’s t-test; for TMT-MS experiment, two-way ANOVA. The statistical details of experiments can be found in the figure legends, including, the name of statistical test, the number of replicates, and exact p values. ’NS’ for p value >0.05, * for p value <0.05, ** for p value <0.01 and *** for p value <0.001. All data points are presented in the figures.

Supplementary Material

Refer to Web version on PubMed Central for supplementary material.

ACKNOWLEDGMENTS

Imaging work was performed at the Northwestern University Center for Advanced Microscopy generously supported by NCI CCSG P30 CA060553 awarded to the Robert H Lurie Comprehensive Cancer Center. This research was supported in part through the computational resources and staff contributions provided for the Quest high-performance computing facility at Northwestern University, which is jointly supported by the Office of the Provost, the Office for Research, and Northwestern University Information Technology. We would like to thank Dr. Rémy Sadoul and Dr. Frank Kirchhoff for sharing *Alix*$^{fl/fl}$ mice with us, Dr. Vincent C. Luca for sharing the Delta^{MAX} plasmids, Dr. Ali Shilatifard, Dr. Fei Chen, and Stacy A. Marshall for helping with RNA sequencing, Dr. Farida Vadimovn a Korobova and Lennell Reynolds Jr for their help with imaging, Dr. Jian Xu and Dr. Toshihiro Nomura for help of vibratome sectioning of mouse hippocampal slices, and Samuel N. Smukowski and David R. Graykowski for technical support. This work was supported by an Individual Biomedical Research Award from The Hartwell Foundation and R01 AG061787 to J.N.S., R01 MH099114 to A.C., and R50 CA221848 to E.T.B., NIH grants AR049867, CA021765, the Assisi Foundation of Memphis, and the American Lebanese Syrian Associated Charities (ALSAC) of SJCRH to A.d’A. A.d’A holds an endowed chair in Genetics and Gene Therapy from the Jewelry Charity Fund. A provisional patent application has been submitted through NU INVO regarding the use of Notch EVs for cell-type-specific cargo delivery.

REFERENCES

1. Budnik V, Ruiz-Cañada C, and Wendler F (2016). Extracellular vesicles round off communication in the nervous system. Nat. Rev. Neurosci. 17, 160–172. [PubMed: 26891626]

2. Wan C, Stowell MHB, and Shen J (2022). Progress and gaps of extracellular vesicle-mediated intercellular cargo transfer in the central nervous system. Commun. Biol. 5, 1223. [PubMed: 36369335]

3. van Niel G, D'Angelo G, and Raposo G (2018). Shedding light on the cell biology of extracellular vesicles. Nat. Rev. Mol. Cell Biol. 19, 213–228. [PubMed: 29339798]

4. Mathieu M, Martin-Jaular L, Lavieu G, and Théry C (2019). Specificities of secretion and uptake of exosomes and other extracellular vesicles for cell-to-cell communication. Nat. Cell Biol. 21, 9–17. [PubMed: 30602770]

5. Kalluri R, and LeBleu VS (2020). The biology, function, and biomedical applications of exosomes. Science 367, eaau6977. [PubMed: 32029601]

6. Pan BT, Teng K, Wu C, Adam M, and Johnstone RM (1985). Electron microscopic evidence for externalization of the transferrin receptor in vesicular form in sheep reticulocytes. J. Cell Biol. 101, 942–948. [PubMed: 2993317]

7. Pastuzyn ED, Day CE, Kearns RB, Kyrke-Smith M, Taibi AV, Mc-Cormick J, Yoder N, Belnap DM, Erlendsson S, Morado DR, et al. (2018). The Neuronal Gene Arc Encodes a Repurposed Retrotransposon Gag Protein that Mediates Intercellular RNA Transfer. Cell 172, 275–288.e18. [PubMed: 29328916]

8. Ashley J, Cordy B, Lucia D, Fradkin LG, Budnik V, and Thomson T (2018). Retrovirus-like Gag Protein Arc1 Binds RNA and Traffics across Synaptic Boutons. Cell 172, 262–274.e11. [PubMed: 29328915]

9. Vilcaes AA, Chanaday NL, and Kavalali ET (2021). Interneuronal exchange and functional integration of synaptobrevin via extracellular vesicles. Neuron 109, 971–983.e5. [PubMed: 33513363]

10. Bahram Sangani N, Gomes AR, Curfs LMG, and Reutelingsperger CP (2021). The role of Extracellular Vesicles during CNS development. Prog. Neurobiol. 205, 102124. [PubMed: 34314775]

11. Fauré J, Lachenal G, Court M, Hirrlinger J, Chatellard-Causse C, Blot B, Grange J, Schoehn G, Goldberg Y, Boyer V, et al. (2006). Exosomes are released by cultured cortical neurones. Mol. Cell. Neurosci. 31, 642–648. [PubMed: 16446100]

12. Chivet M, Javalet C, Laulagnier K, Blot B, Hemming FJ, and Sadoul R (2014). Exosomes secreted by cortical neurons upon glutamatergic synapse activation specifically interact with neurons. J. Extracell. Vesicles 3, 24722. [PubMed: 25398455]

13. Frühbeis C, Fröhlich D, Kuo WP, Amphornrat J, Thilemann S, Saab AS, Kirchhoff F, Möbius W, Goebbels S, Nave KA, et al. (2013). Neurotransmitter-triggered transfer of exosomes mediates oligodendrocyte-neuron communication. PLoS Biol. 11, e1001604. [PubMed: 23874151]

14. Lachenal G, Pernet-Gallay K, Chivet M, Hemming FJ, Belly A, Bodon G, Blot B, Haase G, Goldberg Y, and Sadoul R (2011). Release of exosomes from differentiated neurons and its regulation by synaptic glutamatergic activity. Mol. Cell. Neurosci. 46, 409–418. [PubMed: 21111824]

15. Fitzner D, Schnaars M, van Rossum D, Krishnamoorthy G, Dibaj P, Bakhti M, Regen T, Hanisch UK, and Simons M (2011). Selective transfer of exosomes from oligodendrocytes to microglia by macropinocytosis. J. Cell Sci. 124, 447–458. [PubMed: 21242314]

16. Lu W, Man H, Ju W, Trimble WS, MacDonald JF, and Wang YT (2001). Activation of synaptic NMDA receptors induces membrane insertion of new AMPA receptors and LTP in cultured hippocampal neurons. Neuron 29, 243–254. [PubMed: 11182095]

17. Böing AN, van der Pol E, Grootemaat AE, Coumans FAW, Sturk A, and Nieuwland R (2014). Single-step isolation of extracellular vesicles by size-exclusion chromatography. J. Extracell. Vesicles 3.

18. Kopan R, and Ilagan MXG (2009). The canonical Notch signaling pathway: unfolding the activation mechanism. Cell 137, 216–233. [PubMed: 19379690]

19. Bray SJ (2016). Notch signalling in context. Nat. Rev. Mol. Cell Biol. 17, 722–735. [PubMed: 27507209]

20. Kugeratski FG, Hodge K, Lilla S, McAndrews KM, Zhou X, Hwang RF, Zanivan S, and Kalluri R (2021). Quantitative proteomics identifies the core proteome of exosomes with syntenin-1 as

the highest abundant protein and a putative universal biomarker. Nat. Cell Biol. 23, 631–641. [PubMed: 34108659]

21. Ables JL, Breunig JJ, Eisch AJ, and Rakic P (2011). Not(ch) just development: Notch signalling in the adult brain. Nat. Rev. Neurosci. 12, 269–283. [PubMed: 21505516]
22. Royle SJ, and Lagnado L (2003). Endocytosis at the synaptic terminal. J. Physiol. 553, 345–355. [PubMed: 12963793]
23. Cooney JR, Hurlburt JL, Selig DK, Harris KM, and Fiala JC (2002). Endosomal compartments serve multiple hippocampal dendritic spines from a widespread rather than a local store of recycling membrane. J. Neurosci. 22, 2215–2224. [PubMed: 11896161]
24. Park M, Salgado JM, Ostroff L, Helton TD, Robinson CG, Harris KM, and Ehlers MD (2006). Plasticity-induced growth of dendritic spines by exocytic trafficking from recycling endosomes. Neuron 52, 817–830. [PubMed: 17145503]
25. Schroeter EH, Kisslinger JA, and Kopan R (1998). Notch-1 signalling requires ligand-induced proteolytic release of intracellular domain. Nature 393, 382–386. [PubMed: 9620803]
26. Gonzalez-Perez D, Das S, Antfolk D, Ahsan HS, Medina E, Dundes CE, Jokhai RT, Egan ED, Blacklow SC, Loh KM, et al. (2023). Affinity-matured DLL4 ligands as broad-spectrum modulators of Notch signaling. Nat. Chem. Biol. 19, 9–17. [PubMed: 36050494]
27. Solana-Balaguer J, Campoy-Campos G, Martín-Flores N, Pérez-Sisqués L, Sitjà-Roqueta L, Kucukerden M, Gámez-Valero A, Coll-Manzano A, Martí E, Pérez-Navarro E, et al. (2023). Neuron-derived extracellular vesicles contain synaptic proteins, promote spine formation, activate TrkB-mediated signalling and preserve neuronal complexity. J. Extracell. Vesicles 12, e12355. [PubMed: 37743539]
28. Alberi L, Liu S, Wang Y, Badie R, Smith-Hicks C, Wu J, Pierfelice TJ, Abazyan B, Mattson MP, Kuhl D, et al. (2011). Activity-induced Notch signaling in neurons requires Arc/Arg3.1 and is essential for synaptic plasticity in hippocampal networks. Neuron 69, 437–444. [PubMed: 21315255]
29. Meloty-Kapella L, Shergill B, Kuon J, Botvinick E, and Weinmaster G (2012). Notch ligand endocytosis generates mechanical pulling force dependent on dynamin, epsins, and actin. Dev. Cell 22, 1299–1312. [PubMed: 22658936]
30. Joshi BS, de Beer MA, Giepmans BNG, and Zuhorn IS (2020). Endocytosis of Extracellular Vesicles and Release of Their Cargo from Endosomes. ACS Nano 14, 4444–4455. [PubMed: 32282185]
31. Baietti MF, Zhang Z, Mortier E, Melchior A, Degeest G, Geeraerts A, Ivarsson Y, Depoortere F, Coomans C, Vermeiren E, et al. (2012). Syndecan-syntenin-ALIX regulates the biogenesis of exosomes. Nat. Cell Biol. 14, 677–685. [PubMed: 22660413]
32. Matsui T, Osaki F, Hiragi S, Sakamaki Y, and Fukuda M (2021). ALIX and ceramide differentially control polarized small extracellular vesicle release from epithelial cells. EMBO Rep. 22, e51475. [PubMed: 33724661]
33. Campos Y, Qiu X, Gomero E, Wakefield R, Horner L, Brutkowski W, Han YG, Solecki D, Frase S, Bongiovanni A, and d'Azzo A (2016). Alix-mediated assembly of the actomyosin-tight junction polarity complex preserves epithelial polarity and epithelial barrier. Nat. Commun. 7, 11876. [PubMed: 27336173]
34. Larios J, Mercier V, Roux A, and Gruenberg J (2020). ALIX- and ESCRT-III-dependent sorting of tetraspanins to exosomes. J. Cell Biol. 219, e201904113. [PubMed: 32049272]
35. Matsuo H, Chevallier J, Mayran N, Le Blanc I, Ferguson C, Fauré J, Blanc NS, Matile S, Dubochet J, Sadoul R, et al. (2004). Role of LBPA and Alix in multivesicular liposome formation and endosome organization. Science 303, 531–534. [PubMed: 14739459]
36. Hanson PI, and Cashikar A (2012). Multivesicular body morphogenesis. Annu. Rev. Cell Dev. Biol. 28, 337–362. [PubMed: 22831642]
37. Von Bartheld CS, and Altick AL (2011). Multivesicular bodies in neurons: distribution, protein content, and trafficking functions. Prog. Neurobiol. 93, 313–340. [PubMed: 21216273]
38. Razi M, and Futter CE (2006). Distinct roles for Tsg101 and Hrs in multivesicular body formation and inward vesiculation. Mol. Biol. Cell 17, 3469–3483. [PubMed: 16707569]

39. Laporte MH, Chatellard C, Vauchez V, Hemming FJ, Deloulme JC, Vossier F, Blot B, Fraboulet S, and Sadoul R (2017). Alix is required during development for normal growth of the mouse brain. Sci. Rep. 7, 44767. [PubMed: 28322231]
40. Khan A, Alaamery M, Massadeh S, Obaid A, Kashgari AA, Walsh CA, and Eyaid W (2020). PDCD6IP, encoding a regulator of the ESCRT complex, is mutated in microcephaly. Clin. Genet. 98, 80–85. [PubMed: 32286682]
41. Sun S, Sun L, Zhou X, Wu C, Wang R, Lin SH, and Kuang J (2016). Phosphorylation-Dependent Activation of the ESCRT Function of ALIX in Cytokinetic Abscission and Retroviral Budding. Dev. Cell 36, 331–343. [PubMed: 26859355]
42. Strack B, Calistri A, Craig S, Popova E, and Göttlinger HG (2003). AIP1/ALIX is a binding partner for HIV-1 p6 and EIAV p9 functioning in virus budding. Cell 114, 689–699. [PubMed: 14505569]
43. Soderling TR, and Derkach VA (2000). Postsynaptic protein phosphorylation and LTP. Trends Neurosci. 23, 75–80. [PubMed: 10652548]
44. Laporte MH, Chi KI, Caudal LC, Zhao N, Schwarz Y, Rolland M, Martinez-Hernandez J, Martineau M, Chatellard C, Denarier E, et al. (2022). Alix is required for activity-dependent bulk endocytosis at brain synapses. PLoS Biol. 20, e3001659. [PubMed: 35658004]
45. Naskar S, Narducci R, Balzani E, Cwetsch AW, Tucci V, and Cancedda L (2019). The development of synaptic transmission is time-locked to early social behaviors in rats. Nat. Commun. 10, 1195. [PubMed: 30867422]
46. Farhy-Tselnicker I, and Allen NJ (2018). Astrocytes, neurons, synapses: a tripartite view on cortical circuit development. Neural Dev. 13, 7. [PubMed: 29712572]
47. Breunig JJ, Silbereis J, Vaccarino FM, Sestan N, and Rakic P (2007). Notch regulates cell fate and dendrite morphology of newborn neurons in the postnatal dentate gyrus. Proc. Natl. Acad. Sci. USA 104, 20558–20563. [PubMed: 18077357]
48. Pierfelice T, Alberi L, and Gaiano N (2011). Notch in the vertebrate nervous system: an old dog with new tricks. Neuron 69, 840–855. [PubMed: 21382546]
49. Matsuzaki T, Yoshihara T, Ohtsuka T, and Kageyama R (2019). Hes1 expression in mature neurons in the adult mouse brain is required for normal behaviors. Sci. Rep. 9, 8251. [PubMed: 31160641]
50. Maday S, Twelvetrees AE, Moughamian AJ, and Holzbaur ELF (2014). Axonal transport: cargo-specific mechanisms of motility and regulation. Neuron 84, 292–309. [PubMed: 25374356]
51. Chaumet A, Wright GD, Seet SH, Tham KM, Gounko NV, and Bard F (2015). Nuclear envelope-associated endosomes deliver surface proteins to the nucleus. Nat. Commun. 6, 8218. [PubMed: 26356418]
52. Miaczynska M, Christoforidis S, Giner A, Shevchenko A, Uttenweiler-Joseph S, Habermann B, Wilm M, Parton RG, and Zerial M (2004). APPL proteins link Rab5 to nuclear signal transduction via an endosomal compartment. Cell 116, 445–456. [PubMed: 15016378]
53. Settembre C, Zoncu R, Medina DL, Vetrini F, Erdin S, Erdin S, Huynh T, Ferron M, Karsenty G, Vellard MC, et al. (2012). A lysosome-to-nucleus signalling mechanism senses and regulates the lysosome via mTOR and TFEB. EMBO J. 31, 1095–1108. [PubMed: 22343943]
54. Liu YZ, Zhang H, Zhou DH, Liu YH, Ran XY, Xiang FF, Zhang LN, Chen YJ, Yu XQ, and Li K (2023). Migration from Lysosome to Nucleus: Monitoring Lysosomal Alkalization-Related Biological Processes with an Aminofluorene-Based Probe. Anal. Chem. 95, 7294–7302. [PubMed: 37104743]
55. Zhao Q, Gao SM, and Wang MC (2020). Molecular Mechanisms of Lysosome and Nucleus Communication. Trends Biochem. Sci. 45, 978–991. [PubMed: 32624271]
56. Metz CW, and Bridges CB (1917). Incompatibility of Mutant Races in Drosophila. Proc. Natl. Acad. Sci. USA 3, 673–678. [PubMed: 16586764]
57. Stubbs JD, Lekutis C, Singer KL, Bui A, Yuzuki D, Srinivasan U, and Parry G (1990). cDNA cloning of a mouse mammary epithelial cell surface protein reveals the existence of epidermal growth factor-like domains linked to factor VIII-like sequences. Proc. Natl. Acad. Sci. USA 87, 8417–8421. [PubMed: 2122462]

58. Wang Y, Chan SL, Miele L, Yao PJ, Mackes J, Ingram DK, Mattson MP, and Furukawa K (2004). Involvement of Notch signaling in hippocampal synaptic plasticity. Proc. Natl. Acad. Sci. USA 101, 9458–9462. [PubMed: 15190179]
59. Scannevin RH, and Huganir RL (2000). Postsynaptic organization and regulation of excitatory synapses. Nat. Rev. Neurosci. 1, 133–141. [PubMed: 11252776]
60. Genoud C, Quairiaux C, Steiner P, Hirling H, Welker E, and Knott GW (2006). Plasticity of astrocytic coverage and glutamate transporter expression in adult mouse cortex. PLoS Biol. 4, e343. [PubMed: 17048987]
61. Men Y, Yelick J, Jin S, Tian Y, Chiang MSR, Higashimori H, Brown E, Jarvis R, and Yang Y (2019). Exosome reporter mice reveal the involvement of exosomes in mediating neuron to astroglia communication in the CNS. Nat. Commun. 10, 4136. [PubMed: 31515491]
62. Lee HH, Elia N, Ghirlando R, Lippincott-Schwartz J, and Hurley JH (2008). Midbody targeting of the ESCRT machinery by a noncanonical coiled coil in CEP55. Science 322, 576–580. [PubMed: 18948538]
63. Sherman BT, Hao M, Qiu J, Jiao X, Baseler MW, Lane HC, Imamichi T, and Chang W (2022). DAVID: a web server for functional enrichment analysis and functional annotation of gene lists (2021 update). Nucleic Acids Res. 50, W216–W221. [PubMed: 35325185]
64. Huang DW, Sherman BT, and Lempicki RA (2009). Systematic and integrative analysis of large gene lists using DAVID bioinformatics resources. Nat. Protoc. 4, 44–57. [PubMed: 19131956]
65. Papadopoulos JS, and Agarwala R (2007). COBALT: constraint-based alignment tool for multiple protein sequences. Bioinformatics 23, 1073–1079. [PubMed: 17332019]
66. Eng JK, McCormack AL, and Yates JR (1994). An approach to correlate tandem mass spectral data of peptides with amino acid sequences in a protein database. J. Am. Soc. Mass Spectrom. 5, 976–989. [PubMed: 24226387]
67. Xu T, Park SK, Venable JD, Wohlschlegel JA, Diedrich JK, Cociorva D, Lu B, Liao L, Hewel J, Han X, et al. (2015). ProLuCID: An improved SEQUEST-like algorithm with enhanced sensitivity and specificity. J. Proteomics 129, 16–24. [PubMed: 26171723]
68. Schneider CA, Rasband WS, and Eliceiri KW (2012). NIH Image to ImageJ: 25 years of image analysis. Nat. Methods 9, 671–675. [PubMed: 22930834]
69. Bolger AM, Lohse M, and Usadel B (2014). Trimmomatic: a flexible trimmer for Illumina sequence data. Bioinformatics 30, 2114–2120. [PubMed: 24695404]
70. Anders S, Pyl PT, and Huber W (2015). HTSeq–a Python framework to work with high-throughput sequencing data. Bioinformatics 31, 166–169. [PubMed: 25260700]
71. Robinson MD, McCarthy DJ, and Smyth GK (2010). edgeR: a Bioconductor package for differential expression analysis of digital gene expression data. Bioinformatics 26, 139–140. [PubMed: 19910308]
72. Liu H, and Naismith JH (2008). An efficient one-step site-directed deletion, insertion, single and multiple-site plasmid mutagenesis protocol. BMC Biotechnol. 8, 91. [PubMed: 19055817]
73. Araki Y, Zeng M, Zhang M, and Huganir RL (2015). Rapid dispersion of SynGAP from synaptic spines triggers AMPA receptor insertion and spine enlargement during LTP. Neuron 85, 173–189. [PubMed: 25569349]
74. Morales-Kastresana A, Telford B, Musich TA, McKinnon K, Clayborne C, Braig Z, Rosner A, Demberg T, Watson DC, Karpova TS, et al. (2017). Labeling Extracellular Vesicles for Nanoscale Flow Cytometry. Sci. Rep. 7, 1878. [PubMed: 28500324]
75. Spiegel I, Mardinly AR, Gabel HW, Bazinet JE, Couch CH, Tzeng CP, Harmin DA, and Greenberg ME (2014). Npas4 regulates excitatory-inhibitory balance within neural circuits through cell-type-specific gene programs. Cell 157, 1216–1229. [PubMed: 24855953]
76. Cho JH, Huang BS, and Gray JM (2016). RNA sequencing from neural ensembles activated during fear conditioning in the mouse temporal association cortex. Sci. Rep. 6, 31753. [PubMed: 27557751]
77. Lacar B, Linker SB, Jaeger BN, Krishnaswami SR, Barron JJ, Kelder MJE, Parylak SL, Paquola ACM, Venepally P, Novotny M, et al. (2016). Nuclear RNA-seq of single neurons reveals molecular signatures of activation. Nat. Commun. 7, 11022. [PubMed: 27090946]

78. Weekes MP, Tomasec P, Huttlin EL, Fielding CA, Nusinow D, Stanton RJ, Wang ECY, Aicheler R, Murrell I, Wilkinson GWG, et al. (2014). Quantitative temporal viromics: an approach to investigate host-pathogen interaction. Cell 157, 1460–1472. [PubMed: 24906157]

79. McAlister GC, Nusinow DP, Jedrychowski MP, Wühr M, Huttlin EL, Erickson BK, Rad R, Haas W, and Gygi SP (2014). MultiNotch MS3 enables accurate, sensitive, and multiplexed detection of differential expression across cancer cell line proteomes. Anal. Chem. 86, 7150–7158. [PubMed: 24927332]

80. Ting L, Rad R, Gygi SP, and Haas W (2011). MS3 eliminates ratio distortion in isobaric multiplexed quantitative proteomics. Nat. Methods 8, 937–940. [PubMed: 21963607]

81. Cociorva D, D LT, and Yates JR (2007). Validation of tandem mass spectrometry database search results using DTASelect. Curr Protoc Bioinformatics Chapter 13.

82. Tabb DL, McDonald WH, and Yates JR 3rd. (2002). DTASelect and Contrast: tools for assembling and comparing protein identifications from shotgun proteomics. J. Proteome Res. 1, 21–26. [PubMed: 12643522]

83. Consortium UniProt (2015). UniProt: a hub for protein information. Nucleic Acids Res. 43, D204–D212. [PubMed: 25348405]

84. Raj B, and Blencowe BJ (2015). Alternative Splicing in the Mammalian Nervous System: Recent Insights into Mechanisms and Functional Roles. Neuron 87, 14–27. [PubMed: 26139367]

Highlights

- Excitatory synaptic activity induces the production of EVs containing Notch1 and Notch2
- Notch ligand-receptor system facilitates the specific uptake of EVs by neurons
- EVs trigger the activation of the Notch pathway in recipient neurons
- Alix deletion reduces Notch pathway activation and impairs synaptic protein expression

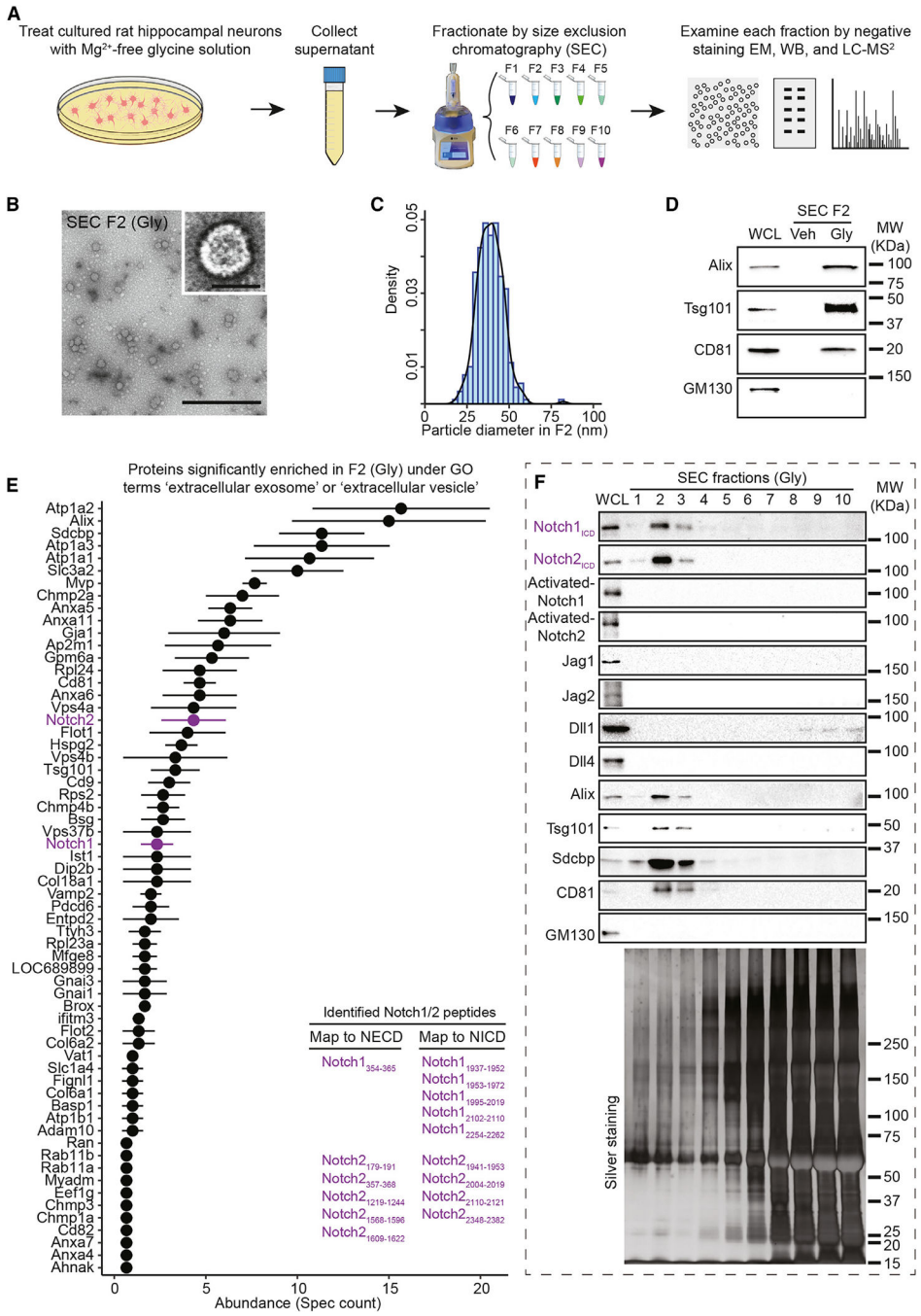

Figure 1. Synaptic NMDAR activation triggers secretion of EVs containing Notch1 and Notch2 proteins

(A) Experimental scheme depicting EV purification workflow and cargo analyses.

(B) Representative images of EV particles present in SEC fraction 2 (F2) visualized by negative staining EM. Scale bar, 500 nm; inset scale bar, 50 nm.

(C) The diameter range of EV-like particles. n = 299 particles from two biological replicates.

(D) The EV markers Alix, Tsg101, and CD81 but not GM130 are selectively detected in SEC F2 isolated from glycine-stimulated neuronal cultures.

(E) Proteomic analysis reveals that Notch1 and Notch2 are highly abundant in SEC F2 along with other known EV protein markers. Mean ± SEM from 3 biological replicates. Insert: Notch1 and Notch2 peptides identified by MS/MS.
(F) WB validation of $Notch1_{ICD}$ and $Notch2_{ICD}$ in SEC F2 (top). Silver-stained gel indicating the total amount of protein loaded across the 10 fractions (bottom). See also Figure S1 and Table S1.

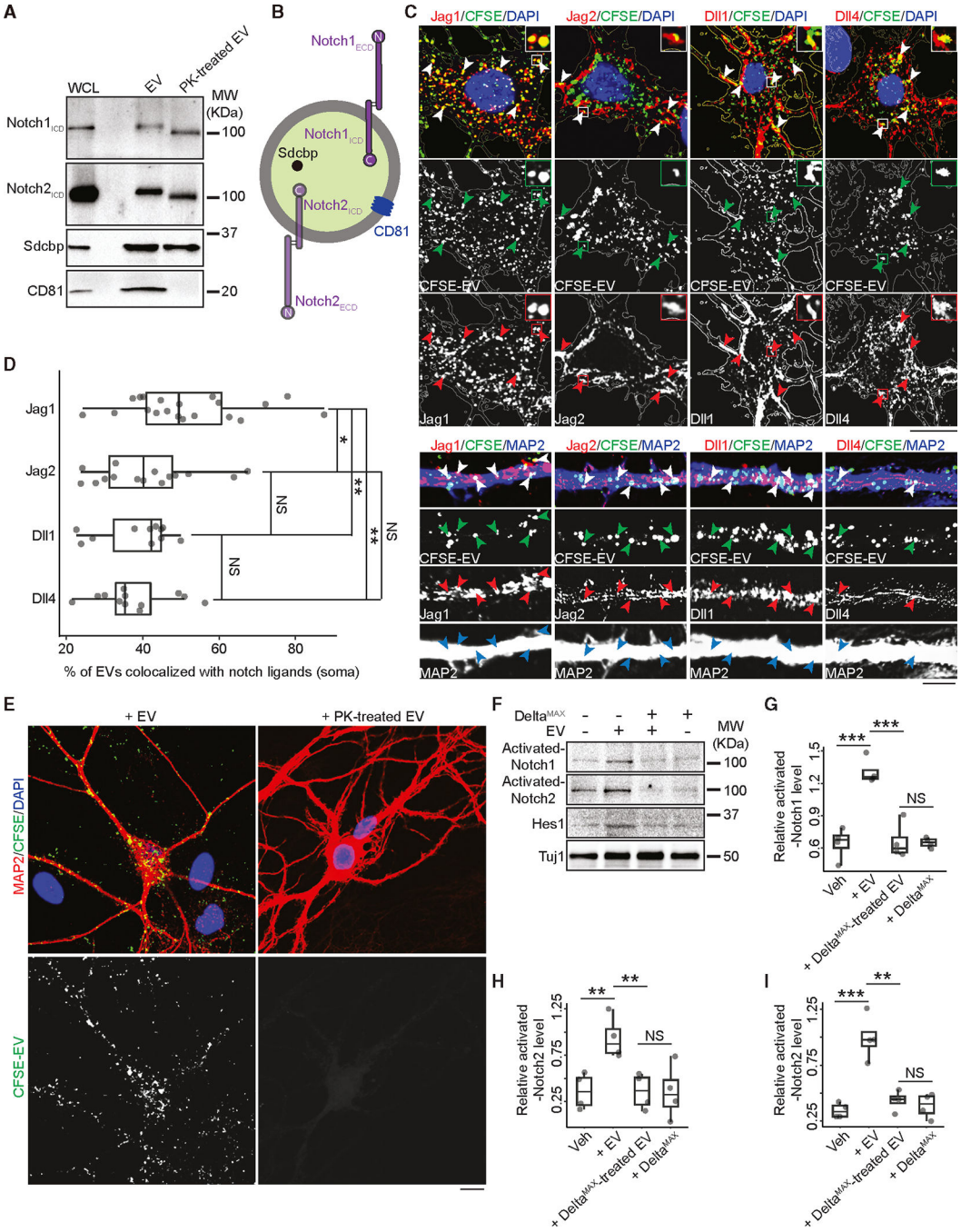

Figure 2. Notch receptor-ligand interactions mediate EV internalization selectively by neurons

(A) Proteinase K (PK) treatment reduces the apparent Notch1 and Notch2 molecular weight by ~10 kDa, consistent with removal of the extracellular portion of $Notch_{ICD}$. No intact CD81 was detected in the PK-treated EVs presumably due to multiple cleavage events, while Sdcbp was unaffected by PK treatment.

(B) Schematic illustrating the arrangement of Notch1, Notch2, CD81, and Sdcbp in EVs.

(C) Representative ICC images showing Notch ligands Jag1, Jag2, Dll1, and Dll4 colocalize with internalized neuronal EVs, labeled with CFSE. Top, neuronal soma, scale bar, 10 μm; bottom, dendrites, scale bar, 5 μm

(D) Quantification of the percentage of CFSE-labeled EVs colocalized with the indicated Notch ligands in neuronal soma. One-tailed Student's t test, n = 12–15 from two cultures. NS, not significant. *p value (Jag1 vs. Jag2) = 0.0204, **p value (Jag1 vs. Dll1) = 0.0082, **p value (Jag1 vs. Dll4) = 0.0051, p value (Jag2 vs. Dll1) = 0.2947, p value (Jag2 vs. Dll4) = 0.2476, p value (Dll1 vs. Dll4) = 0.4396.

(E) Left, CFSE labeled EVs that are internalized by primary cultured rat hippocampal neurons remain generally intact and punctate. Right, neurons fail to internalize PK-treated EVs. Scale bar, 10 μm.

(F) Following a 60-min incubation of primary cultured rat hippocampal neurons with EVs, there is a notable increase in the levels of activated Notch1, activated Notch2, and Hes1 proteins. This effect is not observed with EVs treated with $Delta^{MAX}$ or with $Delta^{MAX}$ treatment alone.

(G–I) Quantifications of (F). One-tailed Student's t test, n = 4 biological. (G) ***p value (Veh vs. EV) = 0.0002, ***p value (EV vs. $Delta^{MAX}$ -treated EV) = 0.0004, NS p value ($Delta^{MAX}$ -treated EV vs. $Delta^{MAX}$) = 0.4453. (H) **p value (Veh vs. EV) = 0.0043, **p value (EV vs. $Delta^{MAX}$-treated EV) = 0.0042, NS p value ($Delta^{MAX}$-treated EV vs. $Delta^{MAX}$) = 0.4927. (I) ***p value (Veh vs. EV) = 0.0004, **p value (EV vs. $Delta^{MAX}$-treated EV) = 0.0011, NS p value ($Delta^{MAX}$ -treated EV vs. $Delta^{MAX}$) = 0.2677. See also Figures S2 and S3.

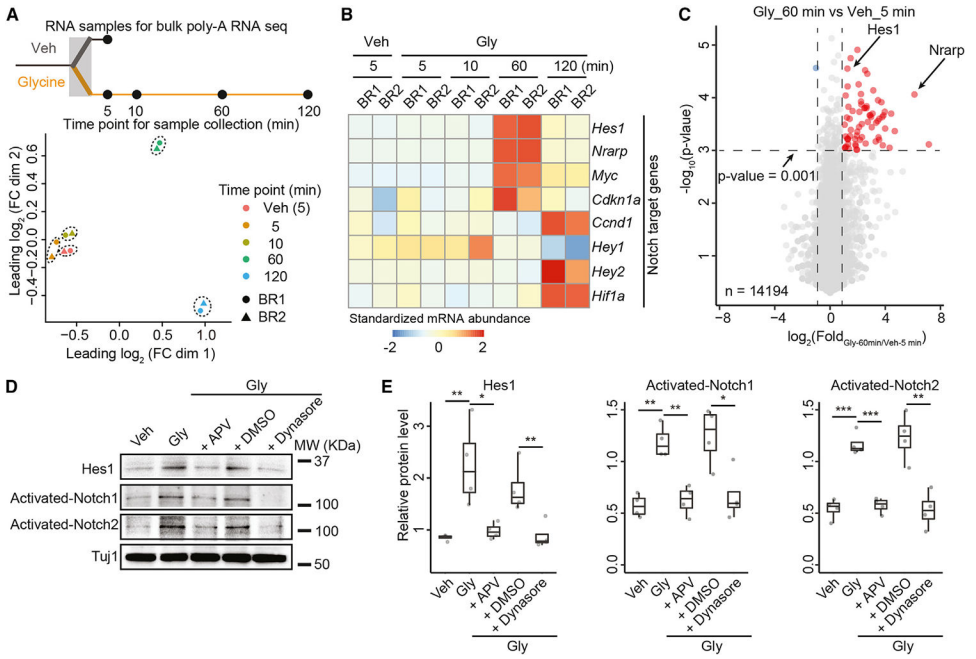

Figure 3. Activation of synaptic NMDARs drives Notch target gene expression

(A) Top, experimental scheme showing the analysis time points for bulk neuron RNA analysis. Bottom, biological replicates cluster by analysis time point in multidimensional scaling plots.

(B) Heatmap showing a panel of Notch target genes that are activated by Mg^{2+}-free glycine treatment.

(C) Volcano plot depicting comparison of mRNA levels in Veh-treated neurons (5 min after treatment) and Mg^{2+}-free glycine-treated neurons (60 min after treatment). One-tailed Student's t test.

(D) Representative WB blot showing Mg^{2+}-free glycine treatment also elevated the levels of activated Notch1, activated Notch2, and Hes1 in primary cultured rat hippocampal neurons (90 min after treatment), which can be inhibited by either D-2-amino-5-phosphonovalerate (APV) or dynasore.

(E) Quantification of (D). n = 4 biological replicates. One-tailed Student's t test. Hes1: **p value (Veh vs. Gly) = 0.0065, *p value (Gly vs. +APV) = 0.0102, **p value (+DMSO vs. +dynasore) = 0.0076. Activated Notch1: **p value (Veh vs. Gly) = 0.0003, **p value (Gly vs. +APV) = 0.0008, *p value (+DMSO vs. +dynasore) = 0.0102. Activated Notch2: ***p value (Veh vs. Gly) = 7.466E-05, ***p value (Gly vs. +APV) = 5.215E-05, **p value (+DMSO vs. +dynasore) = 0.0015. See also Table S2.

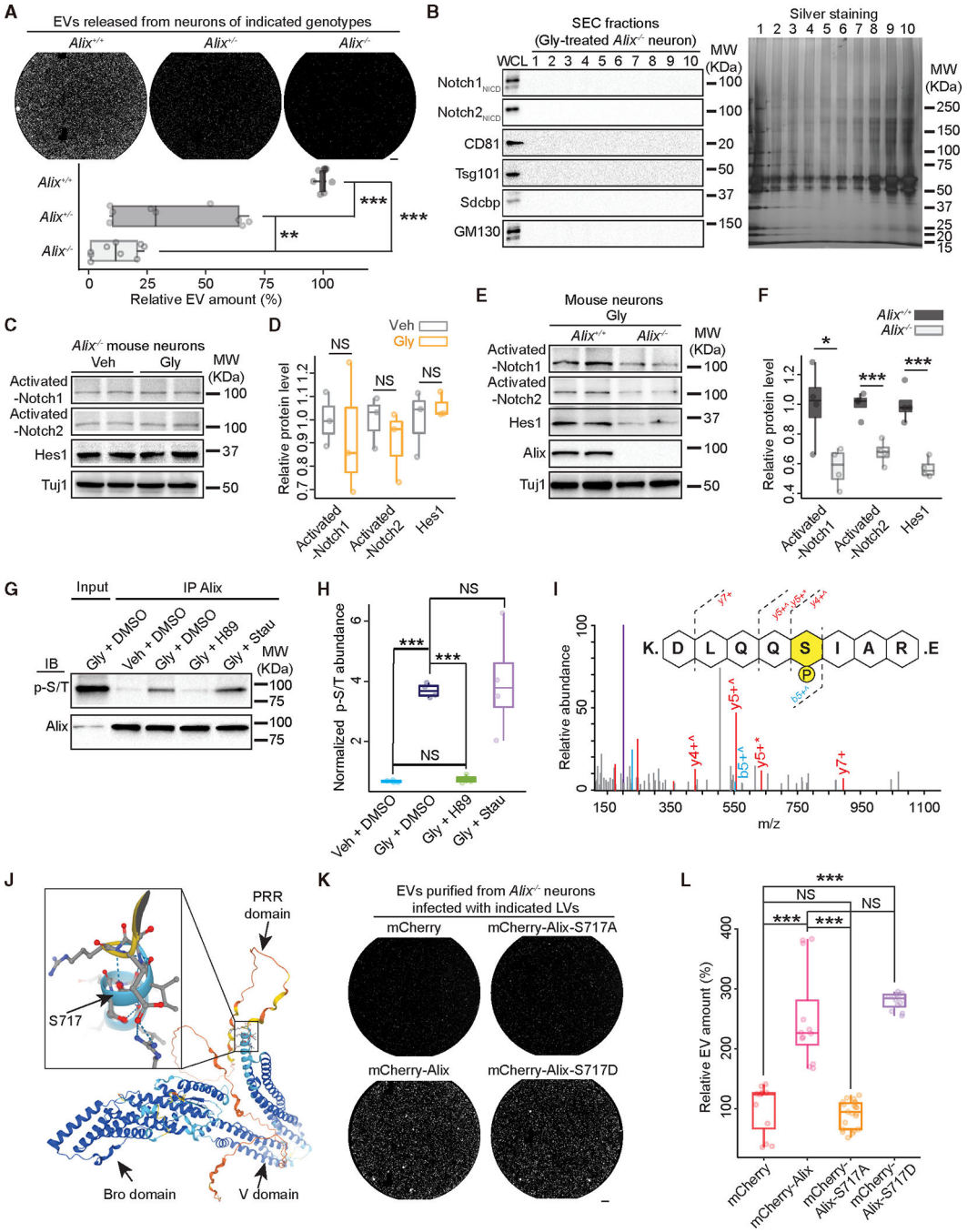

Figure 4. Activation of synaptic NMDARs is insufficient to trigger the Notch EV signaling pathway in *Alix*$^{-/-}$ neurons

(A) Top, representative fluorescent detection of Mg^{2+}-free glycine-induced EVs from neurons with indicated genotypes. Scale bar, 10 μm. Bottom, quantification of Mg^{2+}-free glycine-induced neuronal EVs immunocaptured from indicated neuron genotypes. n = 3 biological replicates (BR). Each chip contains three technical replicates. One-tailed Student's t test. ***p value (*Alix*$^{+/+}$ vs. *Alix*$^{+/-}$) = 7.821-E07, ***p value (*Alix*$^{+/+}$ vs. *Alix*$^{-/-}$) = 3.143-E15, **p value (*Alix*$^{+/-}$ vs. *Alix*$^{-/-}$) = 0.0060.

(B) Left, WB analysis showing Mg^{2+}-free glycine stimulation failed to induce EV release in *Alix*$^{-/-}$ hippocampal neurons. Right, silver-stained gel indicating the total amount of protein recovered across the 10 size exclusion fractions.
(C) WB analysis showing Mg^{2+}-free glycine stimulation failed to upregulate the level of activated Notch1, activated Notch2, and Hes1in *Alix*$^{-/-}$ hippocampal neurons.
(D) Quantification of (C). n = 3 biological replicates. One-tailed Student's t test. NS, not significant. Activated Notch1: p value = 0.3598. Activated Notch2: p value = 0.2162. Hes1: p value = 0.2737.
(E) WB analysis showing Mg^{2+}-free glycine stimulation elevated the levels of activated Notch1, activated Notch2, and Hes1in *Alix*$^{+/+}$ but not *Alix*$^{-/-}$ hippocampal neurons from littermates.
(F) Quantification of (E). n = 4 cultures each genotype. One-tailed Student's t test. Activated-Notch1: *p value = 0.0128. Activated Notch2: ***p value = 0.0007. Hes1, ***p value = 0.0004.
(G) Mg^{2+}-free glycine stimulation leads to Alix phosphorylation, which can be inhibited by PKA inhibitor H89. p-S/T, phosphorylated serine or threonine. Stau, staurosporine.
(H) Quantification of (G). n = 4 biological replicates. One-tailed Student's t test. NS, not significant. ***p value (Veh+DMSO vs. Gly+DMSO) = 1.050E-07, p value (Veh+DMSO vs. Gly+H89) = 0.1624, ***p value (Gly+DMSO vs. Gly+H89) = 2.443E-07, p value (Gly+DMSO vs. Gly+Stau) = 0.3850.
(I) Representative MS^2 spectra indicating Alix phosphorylation at S717 from rat hippocampal neuron whole-cell extracts treated with Mg^{2+}-free glycine. Assigned fragment ions are indicated in b (blue) and y (red), and those containing phosphorylated serine 717 are labeled.
(J) AlphaFold 2-predicted 3D protein structures of rat Alix, indicating the position of S717.
(K) Overexpression of mCherry-Alix or mCherry-Alix-S717D rescues Mg^{2+}-free glycine-induced EV release from *Alix*$^{-/-}$ neurons. Scale bar, 10 μm.
(L) Quantification of (K). n = 4–7 biological replicates. Each chip contains three technical replicates. One-tailed Student's t test. NS, not significant. ***p value (mCherry vs. mCherry-Alix) = 4.249E-06, p value (mCherry vs. mCherry-Alix-S717A) = 0.2110, ***p value (mCherry vs. mCherry-Alix-S717D) = 6.004E-13, ***p value (mCherry-Alix vs. mCherry-Alix-S717A) = 5.468E-10, p value (mCherry-Alix vs. mCherry-Alix-S717D) = 0.1312. See also Figures S4 and S5 and Table S3.

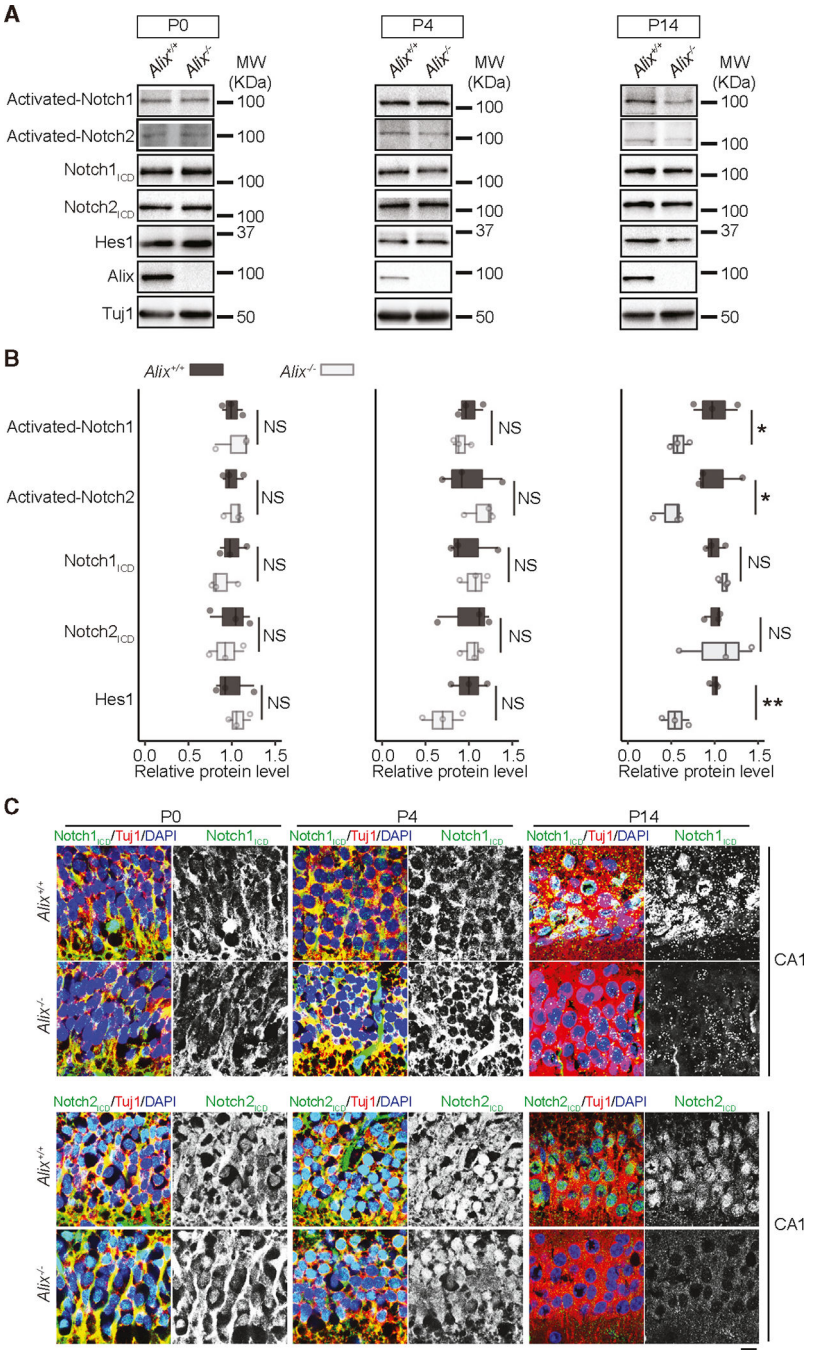

Figure 5. Stunted Notch pathway in hippocampus of juvenile *Alix*$^{-/-}$ mouse

(A) WB analyses showing that, at P0 and P4, the levels of activated Notch1, activated Notch2, $Notch1_{ICD}$, $Notch2_{ICD}$, and Hes1 are similar in *Alix*$^{+/+}$ and *Alix*$^{-/-}$ hippocampi. However, at P14, the levels of activated Notch1, activated Notch2, and Hes1 are significantly reduced in *Alix*$^{-/-}$ hippocampus.

(B) Quantification of (A). n = 3 mice for each group. One-tailed Student's t test, NS, not significant. P0: activated Notch1 p value = 0.3752, activated Notch2 p value = 0.3865, $Notch1_{ICD}$ p value = 0.2047, $Notch2_{ICD}$ p value = 0.3590, Hes1 p value = 0.1232. P4:

activated Notch1 p value = 0.2149, activated Notch2 p value = 0.2743, $Notch1_{ICD}$ p value = 0.3837, $Notch2_{ICD}$ p value = 0.4283, Hes1 p value = 0.0836. P14: activated Notch1 *p value = 0.0324, activated Notch2 *p value = 0.0265, $Notch1_{ICD}$ p value = 0.1029, $Notch2_{ICD}$ p value = 0.4227, Hes1 **p value = 0.0042.

(C) At P0 and P4, the expression patterns of $Notch1_{ICD}$ and $Notch2_{ICD}$ are similar in $Alix^{+/+}$ and $Alix^{-/-}$ hippocampal CA1 regions. At P14, the amounts of nuclear-localized $Notch1_{ICD}$ and $Notch2_{ICD}$ are much less in $Alix^{-/-}$ hippocampal CA1 regions compared to $Alix^{+/+}$ hippocampus. Scale bar, 10 μm. See also Figure S6.

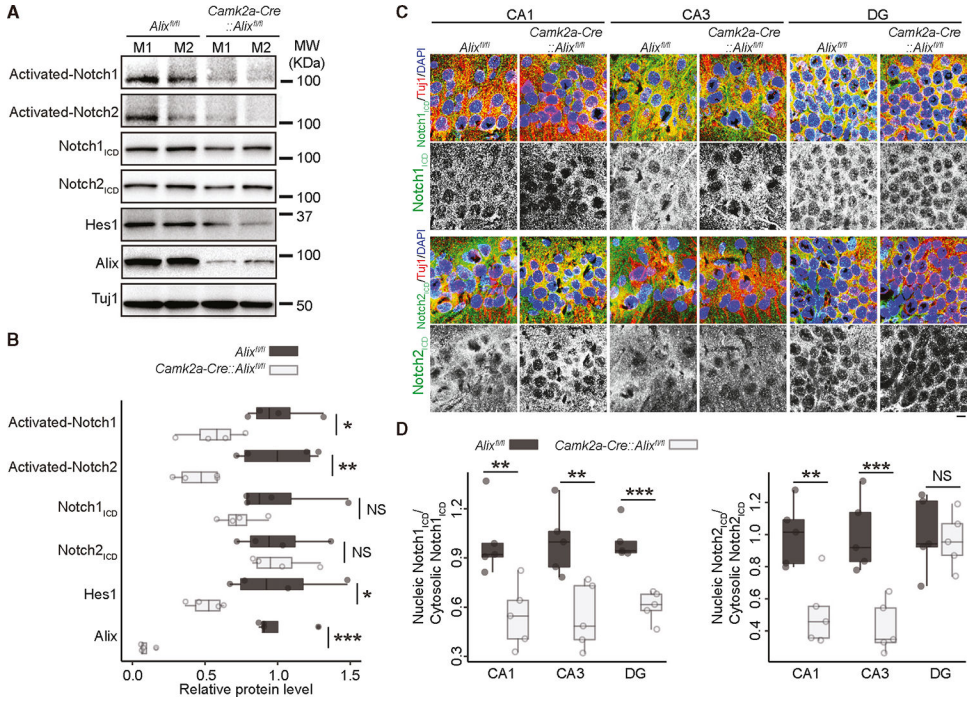

Figure 6. Conditional deletion of Alix in adult mouse hippocampus reduces Notch signaling pathway activation

(A) The levels of activated Notch1, activated Notch2, and Hes1 are significantly reduced in hippocampus from ~2-month-old *Camk2a-cre*::*Alix* $^{fl/fl}$ mice compared to *Alix* $^{fl/fl}$ mice. M = mouse.

(B) Quantification of (A). n = 4 mouse per group. One-tailed Student's t test. NS, not significant. Activated Notch1: *p value = 0.0143, activated Notch2: **p value = 0.0075, $Notch1_{ICD}$: p value = 0.0942, $Notch2_{ICD}$: p value = 0.4709, Hes1: *p value = 0.0218, Alix: ***p value = 5.346E-05.

(C) Lack of Alix in adult hippocampus led to alteration of nuclear-localized $Notch1_{ICD}$ and $Notch2_{ICD}$. Scale bar, 10 μm

(D) Quantification of (C). n = 5 mouse per group. One-tailed Student's t test. NS, not significant. Nucleic $Notch1_{ICD}$/cytosolic $Notch1_{ICD}$: CA1, **p value = 0.0042, CA3, **p value = 0.0037, DG, ***p value = 0.0002. Nucleic $Notch2_{ICD}$/cytosolic $Notch2_{ICD}$: CA1, **p value = 0.0026, CA3, ***p value = 0.0009, DG, p value = 0.3942.

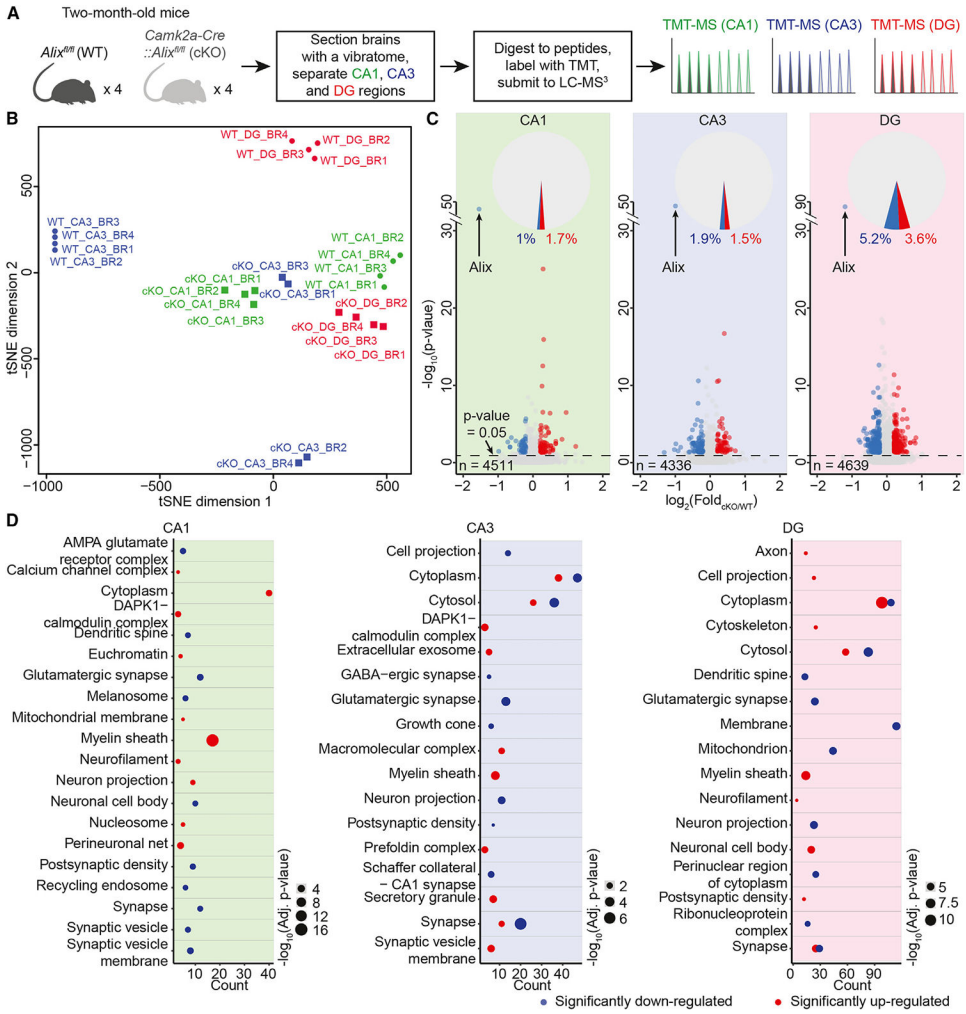

Figure 7. Conditional deletion of Alix in adult mouse hippocampus disrupts glutamatergic synapse protein expression

(A) Experimental design to examine subregion-specific proteomic differences in the hippocampus between *Camk2a-cre::Alix* $^{fl/fl}$ and *Alix* $^{fl/fl}$ mice.

(B) The t-SNE (t-distributed stochastic neighbor embedding) plot illustrates dissimilar protein expression in of all samples. BR, biological replicate.

(C) Volcano plots depicting comparison of *Camk2a-cre::Alix*$^{fl/fl}$ and *Alix*$^{fl/fl}$ hippocampal subregion-specific proteomes. n = 4 mice per experimental group. Pie charts summarizing proteins differently expressed by WT and cKO mice in each hippocampal region. Two-way ANOVA.

(D) GO::CC gene annotation analysis suggests lack of Alix expression in adult hippocampus mainly affects glutamatergic synapses in CA1, CA3, and DG. List of the top 10 most significantly enriched terms for both significantly down- and upregulated proteins. See also Figure S7 and Table S4.

KEY RESOURCES TABLE

REAGENT or RESOURCE	SOURCE	IDENTIFIER
Antibodies		
Chicken anti-MAP2	Millipore Sigma	Cat#AB5543; RRID: AB_571049
Mouse anti-Jag1	Santa Cruz Biotechnology	Cat# sc-390177; RRID: AB_2892141
Goat anti-Jag2	Thermo Fisher Scientific	Cat# PA5–47188; RRID: AB_2576459
Rabbit anti-Jag2	Cell Signaling Technology	Cat# 2210; RRID: AB_823553
Goat anti-Dll1	Abcam	Cat# ab85346; RRID: AB_1860332
Rabbit anti-DiM	Cell Signaling Technology	Cat# 2588; RRID: AB_2292961
Goat anti-Dll4	Thermo Fisher Scientific	Cat# PA5–46974; RRID: AB_2577158
Rabbit anti-Dll4	Cell Signaling Technology	Cat# 96406; RRID: AB_2800263
Guinea pig anti-VGluTI	Millipore Sigma	Cat# AB5905; RRID: AB_2301751
Rabbit anti-Homer1	Synaptic Systems	Cat# 160 003; RRID: AB_887730
Mouse anti-Tsg101	Santa Cruz Biotechnology	Cat# sc-7964; RRID: AB_671392
Rabbit anti-Notch2$_{ICD}$	Abcam	Cat# ab52627; RRID: AB_881725
Rabbit anti-activated Notch1	Abcam	Cat# ab52301; RRID: AB_881726
Rabbit anti-Notch2$_{ICD}$	Cell Signaling Technology	Cat# 5732; RRID: AB_10693319
Rabbit anti-activated Notch2	MyBioSource	Cat# MBS9410510
Mouse anti-PSD95	Thermo Fisher Scientific	Cat# MA1–046; RRID: AB_2092361
Rabbit anti-PSD95(pS295)	Abcam	Cat# ab76108; RRID: AB_1310621
Mouse anti-Alix	Cell Signaling Technology	Cat# 2171; RRID: AB_2299455
Rabbit anti-Alix	Cell Signaling Technology	Cat# 18269; RRID: AB_2798796
Mouse anti-CD81	Santa Cruz Biotechnology	Cat# sc-166029; RRID: AB_2275892
Rabbit anti-Sdcbp	Abcam	Cat# ab19903; RRID: AB_445200
Rabbit anti-Sdcbp	Cell Signaling Technology	Cat # 27964
Mouse anti-LBPA	Millipore Sigma	Cat # MABT837
Rabbit anti-GM130	Abcam	Cat# ab52649; RRID: AB_880266
Rabbit anti-Hes1	Cell Signaling Technology	Cat# 11988; RRID: AB_2728766
Rabbit anti-Hes1	Abcam	Cat# ab71559; RRID: AB_1209570
Chicken anti-Tuj1	Novus Biologicals	Cat# NB100–1612; RRID: AB_10000548
Rabbit anti-p-S/T	Cell Signaling Technology	Cat# 9624; RRID: AB_331817
Rabbit anti-GAPDH	Cell Signaling Technology	Cat# 2118; RRID: AB_561053
Chicken anti-GFP	Abcam	Cat# ab13970; RRID: AB_300798
Mouse anti-myc	Santa Cruz Biotechnology	Cat# sc-40; RRID: AB_627268
Rabbit anti-GluA1	EMD Millipore	Cat# PC246; RRID: AB_564636
Guinea pig anti-Bassoon	Synaptic Systems	Cat# 141 318; RRID: AB_2927388
Goat anti-Mouse IgG (H + L) Highly Cross-Adsorbed Secondary Antibody, Alexa Fluor 488	Thermo Scientific	Cat# A-11029; RRID: AB_2534088
Donkey anti-Goat IgG (H + L) Cross-Adsorbed Secondary Antibody, Alexa Fluor 568	Thermo Scientific	Cat# A-11057; RRID: AB_2534104
Donkey anti-Mouse IgG (H + L) Highly Cross-Adsorbed Secondary Antibody, Alexa Fluor 568	Thermo Scientific	Cat# A10037; RRID: AB_2534013

REAGENT or RESOURCE	SOURCE	IDENTIFIER
Goat anti-Rabbit IgG (H + L) Cross-Adsorbed Secondary Antibody, Alexa Fluor 568	Thermo Scientific	Cat# A-11011 (also A11011); RRID: AB_143157
Donkey anti-Goat IgG (H + L) Cross-Adsorbed Secondary Antibody, Alexa Fluor 488	Thermo Scientific	Cat# A-11055 (also A11055); RRID: AB_2534102
Goat anti-Chicken IgY (H + L) Secondary Antibody, Alexa Fluor 555	Thermo Scientific	Cat# A-21437; RRID: AB_2535858
Goat anti-Rabbit IgG (H + L) Highly Cross-Adsorbed Secondary Antibody, Alexa Fluor 488	Thermo Scientific	Cat# A-11034 (also A11034); RRID: AB_2576217
Goat Anti-Guinea pig IgG H&L (Alexa Fluor 647)	Abcam	Cat# ab150187; RRID: AB_2827756
Goat anti-Rabbit IgG (H + L) Poly-HRP Secondary Antibody, HRP	Thermo Scientific	Cat# 32260; RRID: AB_1965959
Goat anti-Mouse IgG (H + L) Poly-HRP Secondary Antibody, HRP	Thermo Scientific	Cat# 32230; RRID: AB_1965958
Goat anti-Chicken IgY H&L (HRP) secondary antibody	Abcam	Cat# ab97135; RRID: AB_10680105
IgG(H + L) Goat anti-Guinea Pig, HRP, Polyclonal, Southern Biotech	Fisher Scientific	Cat# OB6090–05
Bacterial and virus strains		
pz196-mCherry	Dr. Evangelos Kiskinis lab	N/A
pz196-mCherry-Alix	Dr. Evangelos Kiskinis lab	N/A
pz196-mCherry-Alix-S717A	Dr. Evangelos Kiskinis lab	N/A
pz196-mCherry-Alix-S717D	Dr. Evangelos Kiskinis lab	N/A
pz196-Notch1-myc	Dr. Evangelos Kiskinis lab	N/A
Chemicals, peptides, and recombinant proteins		
Hank's Balanced Salt Solution	Thermo Fisher Scientific	Cat# 14170112
EV-free PBS	MEDIATECH INC CA	Cat# 21–040-CV
D-PBS	Fisher Scientific	Cat# AAJ67802K2
Lambda phosphatase	New England Biolabs	Cat# P0753S
Poly-D-lysine	Fisher Scientific	Cat# CB-40210
Laminin	Fisher Scientific	Cat# 23–017-015
SM1	STEMCELL Technologies	Cat# 05711
5-fluoro-2-deoxyuridine	Sigma-Aldrich	Cat# F0503
Uridine	Sigma-Aldrich	Cat# U6381
NaCl	Sigma-Aldrich	Cat# S7653
KCl	Sigma-Aldrich	Cat# P9333
NaH_2PO_4	Sigma-Aldrich	Cat# 71505
$NaHCO_3$	Sigma-Aldrich	Cat# S6014
Glucose	Sigma-Aldrich	Cat# G7021
CaCl2	Sigma-Aldrich	Cat# C1016
MgCl2	Sigma-Aldrich	Cat# M8266
CsF	Sigma-Aldrich	Cat# 198323
CsCl	Sigma-Aldrich	Cat# 289329
HEPES	Sigma-Aldrich	Cat# H3375
EGTA	DOT Scientific Inc	Cat# DSE57060

REAGENT or RESOURCE	SOURCE	IDENTIFIER
Mg-ATP	Sigma-Aldrich	Cat# A9187
QX-314	Sigma-Aldrich	Cat# 552233
TEA-Cl	Sigma-Aldrich	Cat# 86614
4-AP	Sigma-Aldrich	Cat# 275875
CsOH	Sigma-Aldrich	Cat# C8518
TTX	Fisher Scientific	Cat# NC0738940
Picrotoxin	Sigma-Aldrich	Cat# P1675
Bicuculline	Sigma-Aldrich	Cat# 14340
Glycine	Sigma-Aldrich	Cat# G5417
Strychnine	Sigma-Aldrich	Cat# S0532
CFSE	Thermo Fisher Scientific	Cat# C34554
CM-Dil	Thermo Fisher Scientific	Cat# C7000
DMSO	Sigma-Aldrich	Cat# D2650
Proteinase K	Fisher Scientific	Cat# NC0547027
PFA	Fisher Scientific	Cat# AAA1131336
Triton X-100	Sigma-Aldrich	Cat# X100
DAPI	Sigma-Aldrich	Cat# D9542
Fluoromount-G	Southern Biotech	Cat# 0100–01
Dynasore	Sigma-Aldrich	Cat# SML0340
H89	Sigma-Aldrich	Cat# B1427
Staurosporine	Tocris	Cat# 1285
APV	Sigma-Aldrich	Cat# A5282
KN93	Sigma-Aldrich	Cat# K1385
AIP	Anaspec	Cat# AS-64929
Trizma base	Sigma-Aldrich	Cat# RDD008
SDS	DOT Scientific Inc	Cat# DSL22040
EDTA	DOT Scientific Inc	Cat# DS170184
Sodium deoxycholate	Sigma-Aldrich	Cat# D6750
Protease inhibitor cocktail	Thermo Fisher Scientific	Cat# 78443
Phosphatase inhibitor	Thermo Fisher Scientific	Cat# 78420
BSA	Jackson immunoResearch laboratories,	Cat# 001–000-162
Tween 20	DOT Scientific Inc	Cat# DSP20370–4
Tris-Cl	Sigma-Aldrich	Cat# T5941
NaF	Sigma-Aldrich	Cat# S7920
β-glycerophosphate	Sigma-Aldrich	Cat# G9422
Sodium orthovanadate	Sigma-Aldrich	Cat# 450243
N-ethylmaleimide	Sigma-Aldrich	Cat# E3876
Protein G Sepharose 4 Fast Flow	Thermo Fisher	Cat# 45–000-116
IgG	Sigma-Aldrich	Cat# 15381
Dithiothreitol	DOT Scientific Inc	Cat# DSD11000
$MnCl_2$	Sigma-Aldrich	Cat# M8266

REAGENT or RESOURCE	SOURCE	IDENTIFIER
Embedding medium	Sakura	Cat# 4583
ProLong Diamond Antifade Mountant	Thermo Fisher Scientific	Cat# P36970
Trichloroacetic acid	Sigma-Aldrich	Cat# T0699
Urea	Thermo Fisher Scientific	Cat# 29700
NH_4HCO_3	Fluka	Cat# 09830
Iodoacetamide	Sigma-Aldrich	Cat# I1149
Lys-C	Thermo Fisher Scientific	Cat# 90307_3668048707
Trypsin	Promega	Cat# V5280
Trifluoroacetic acid	Fisher Scientific	Cat# O4902–100
Acetonitrile	Fisher Scientific	Cat# A955–212
Hydroxylamine	Sigma-Aldrich	Cat# 467804
$Delta^{MAX}$	GenScript & Dr. Vincent Luca lab, Gonzalez-Perez et al.[26]	Custom synthesis
Critical commercial assays		
ExoView Mouse Tetraspanin chip with ExoView Tetraspanin kit	Nanoview Bioscience	Cat# EV-TETRA-M2
LDH assay kit	Thermo Fisher Scientific	Cat# 88953
HilyMax	Dojindo	Cat# H357–15
RNeasy mini Kit	Qiagen	Cat# 74104
RiboZero kit	Epicentre	Cat# MRZH116
Oligo(dT) magnetic beads	Thermo	Cat# 61002
BCA	Thermo Fisher Scientific	Cat# 23225
Pierce Silver Stain Kit	Thermo Fisher	Cat# 24612
ZipTip	Thermo Fisher-Pierce	Cat# 87784
High-Select™ TiO2 Phosphopeptide Enrichment Kit	Thermo Fisher Scientific	Cat# A32993
Micro BCA kit	Fisher Scientific	Cat# PI23235
TMT	Thermo Fisher Scientific	Cat# 44520
High pH reverse-phase peptide fractionation kit	Thermo Fisher Scientific	Cat# 84868
Deposited data		
Bulk RNA sequencing data	This study	GEO: GSE110908,https://www.ncbi.nlm.nih.gov/geo/query/acc.cgi?acc=GSE110908
Mass spectrometry data	This study	MassIVE: MSV000093592,https://massive.ucsd.edu/ProteoSAFe/dataset.jsp?task=50acc1d7e2694135b19df30ef1a82161 ProteomeXchange: PXD047597, https://proteomecentral.proteomexchange.org/cgi/GetDataset?ID=PXD047597
Experimental models: Organisms/strains		
Wistar rat	Charles River	273
Alix$^{+/-}$ mice	Dr. Alessandra d'Azzo lab[33]	N/A

REAGENT or RESOURCE	SOURCE	IDENTIFIER
Alix$^{fl/fl}$ mice	Dr. Rémy Sadoul and Dr. Frank Kirchhoff lab[39]	N/A
Camk2a-Cre mice	The Jackson Laboratory	005359
Oligonucleotides		
AlixS717A_For: acttgcaacaaGCAattgccagagaacctagtgct	This study	N/A
AlixS717A_Rev: gttctctggcaatTGCttgttgcaagtcctttaag	This study	N/A
AlixS717D_For: acttgcaacaaGATattgccagagaacctagtgct	This study	N/A
AlixS717D_Rev: gttctctggcaatATCttgttgcaagtcctttaag	This study	N/A
Recombinant DNA		
mCherry-Alix	Addgene/James Hurley lab, Lee et al.[62]	Cat# 21504; RRID:Addgene_21504
GFP	Dr. Peter Penzes lab	N/A
mCherry	Dr. Peter Penzes lab	N/A
pz196	Dr. Evangelos Kiskinis lab	N/A
Notchl-myc	Addgene/Raphael Kopan lab, Schroeter et al.[25]	Cat# 41728; RRID:Addgene_41728
mCherry-Alix-S717A	This study	N/A
mCherry-Alix-S717D	This study	N/A
Software and algorithms		
Spyder	MIT	https://www.spyder-ide.org/
RStudio	Posit PBC	https://posit.co/products/open-source/rstudio/
DAVID	NIH, Sherman et al.[63] and Huang et al.[64]	https://david.ncifcrf.gov
COBALT	NIH, Papadopoulos & Agarwala[65]	https://www.ncbi.nlm.nih.gov/tools/cobalt/re_cobalt.cgi
NCBI Multiple Sequence Alignment Viewer	NIH	https://www.ncbi.nlm.nih.gov/projects/msaviewer/
IP2	Bruker, Eng et al.[66] and Xu et al.[67]	http://www.integratedproteomics.com
Fiji	NIH, Schneider et al.[68]	https://fiji.sc/
ExoView Analyzer 3.1.4	Nanoview Bioscience	https://www.accela.eu/nanoview-biosciences
pClamp 10.7	Axon Instruments	https://support.moleculardevices.com/s/
miniAnalysis	Bluecell	http://bluecell.co.kr/theme/theme05/product/product_02_01.php
FastQC	QUBES	https://qubeshub.org/resources/fastqc
Trimmomatic	THE USADEL LAB, Bolger et al.[69]	http://www.usadellab.org/cms/?page=trimmomatic
TopHat	Transcriptomics technologies	https://ccb.jhu.edu/software/tophat/index.shtml
HTseq	Dr. Simon Anders lab, Anders et al.[70]	https://htseq.readthedocs.io/en/latest/
EdgeR	Bioconductor, Robinson et al.[71]	https://bioconductor.org/packages/release/bioc/html/edgeR.html
Imaris 10.0.0	Oxford Instruments	https://imaris.oxinst.com/

REAGENT or RESOURCE	SOURCE	IDENTIFIER
Other		
Tecnai Spirit G2 120 kV transmission EM	FEI	N/A
Multiclamp700B amplifier	Axon Instruments Inc.	N/A
Cover glasses	Carolina	Cat# 633037
NanoView R100	Nanoview Bioscience	N/A
MWCO filter, 10 kDa	EMD Millipore	Cat# UFC801024
MWCO filter, 30 kDa	Millipore Sigma	Cat# MRCF0R030
qE-Voriginal-35nm SEC column	Izon Science	Cat# SP5-USD
Automated fraction collector V1	Izon Science	Cat# AFC-V1
Synergy HTX multi-mode microplate reader	Biotek	N/A
Magnetic imaging chamber	Warner Instruments	Cat# QR-40L
A1R + confocal laser microscope	Nikon	N/A
Electronic homogenizer	Glas-Col	Cat# 099C-K54
WedgeWell™ Tris-Glycine Mini Protein Gels	Fisher Scientific	Cat# XP04125BOX, XP04120BOX and XV00100PK20
Nitrocellulose membranes	Thermo Fisher	Cat# 4500002
Chemidoc XRS system	Bio-Rad	N/A
HyperSep C18 Cartridges	ThermoFisher Scientific	Cat# 60108–302
Peptide Desalting Spin Columns	Thermo Fisher Scientific	Cat# 89852
UltiMate 3000 HPLC pump	Thermo Scientific	N/A
NanoViper Trap Column	Thermo Fisher Scientific	Cat# 164535
NanoViper analytical column	Thermo Fisher Scientific	Cat# 164570
Orbitrap Fusion	Thermo Fisher Scientific	N/A